AMERICAN UNIVERSITY OF BEIRUT

THE PERIVASCULAR ADIPOCYTE: A CROOKED MIDDLEMAN IN THE TRANSLATION OF METABOLIC CHALLENGE INTO EARLY VASCULAR DYSFUNCTION

by
RIM WASSIM RAFEH

A thesis
submitted in partial fulfillment of the requirements
for the degree of Master of Science
to the Department of Pharmacology and Toxicology
of the Faculty of Medicine
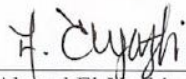at the American University of Beirut

Beirut, Lebanon
May 2019

AMERICAN UNIVERSITY OF BEIRUT

THE PERIVASCULAR ADIPOCYTE: A CROOKED
MIDDLEMAN IN THE TRANSLATION OF METABOLIC
CHALLENGE INTO EARLY VASCULAR DYSFUNCTION

By

RIM WASSIM RAFEH

Approved by:

_____
Dr. Ahmed El-Yazbi, Assistant Professor   Advisor
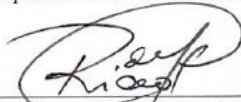Department of Pharmacology and Toxicology

_____
Dr. Ali Eid, Assistant Professor   Co-Advisor
Department of Pharmacology and Toxicology
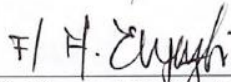
_____
Dr. Ramzi Sabra, Professor and Chairperson   Member of Committee
Department of Pharmacology and Toxicology

_____
Dr. Riyad El-Khoury, Assistant Professor   Member of Committee
Department of Pathology and Laboratory Medicine

_____
Dr. Damon Poburko, Associate Professor   Member of Committee
Department of Biomedical Physiology and Kinesiology
Simon Fraser University

May 20th, 2019

AMERICAN UNIVERSITY OF BEIRUT

THESIS RELEASE FORM

Student Name: __Rafeh_____Rim_____Wassim_____
                   Last   First   Middle

I authorize the American University of Beirut, to: (a) reproduce hard or electronic copies of my thesis; (b) include such copies in the archives and digital repositories of the University; and (c) make freely available such copies to third parties for research or educational purposes:

☐ As of the date of submission

☒ One year from the date of submission of my thesis.

☐ Two years from the date of submission of my thesis.

☐ Three years from the date of submission of my thesis.

_____August 28th,2021_____

Signature   Date

ACKNOWLEDGEMENTS

ABSTRACT
OF THE THESIS OF

Rim Wassim Rafeh   for   Master of Science
                                       Major: Pharmacology and Therapeutics

Title: The Perivascular Adipocyte: A Crooked Middleman In The Translation Of Metabolic Challenge Into Early Vascular Dysfunction

Cardiovascular disease is the leading cause of morbidity and mortality among diabetic patients. Although prolonger exposure to hyperglycemia is implicated in the pathogenesis of cardiovascular dysfunction, a significant proportion of patients display established diabetic microvascular complications at initial diagnosis of diabetes, before overt hyperglycemia. Moreover, recent studies from our laboratory have shown that cardiovascular dysfunction is evident in animal models of metabolic challenge before the onset of hyperglycemia and diabetes, thus placing the etiology of this early cardiovascular dysfunction in question.

Given the role of adipose tissue inflammation in the pathophysiology of metabolic syndrome, we hypothesized that interaction between perivascular adipose tissue and vascular smooth muscle cells may play a role in early cardiovascular dysfunction.

Phenotypic characteristics (migration, proliferation, metabolic activity, and protein marker expression) of primary aortic vascular smooth muscle cells (VSMCs) will be examined in control and prediabetic rats. The effect of exposure of control VSMCs to elevated insulin and free fatty acid (FFA) concentrations, mimicking the serum environment in prediabetic rats, will be assessed and compared to the observed phenotype of prediabetic VSMCs. To investigate the role of adipocytes in mediating VSMC dysfunction, 3T3-L1 cells will be differentiated to adipocyte-like cells and exposed to the above insulin and FFA treatment. The conditioned media from these cells will be used to treat control VSMCs to see if the prediabetic phenotype will be recapitulated. A human counterpart to this model will be used, as well, via the differentiation of human bone marrow mesenchymal stem cells into adipocyte-like cells, and challenging with insulin and FFAs. The conditioned medium will be used to treat human subcutaneous VSMCs, whose phenotype will be investigated. Control and challenged VSMC and adipocyte interaction with the immune system will be assessed through monocyte recruitment assays using THP-1. An attempt to resolve the identity and the effect of soluble mediators produced in the conditioned media will be made via western blotting and/or pharmacological blockers.

We expect that the metabolic challenge will alter VSMC phenotype indirectly via evoking pro-inflammatory changes in adipocytes. The latter, in turn, will produce soluble mediators that have direct effects on VSMCs.

TABLE OF CONTENTS

ILLUSTRATIONS

Figure

ABBREVIATIONS

BAT: Brown adipose tissue

CVD: Cardiovascular disease

DM: Diabetes mellitus

HC: Hypercaloric

HFD: High-fat diet

IGT: Impaired glucose tolerance

MHC: Mild hypercaloric

PVAT: Perivascular adipose tissue

UCP-1: Uncoupling protein 1

VSMC: Vascular smooth muscle cell

WAT: White adipose tissue

CHAPTER I

INTRODUCTION

A. Diabetes Mellitus: A Hyperglycemic Endpoint to a Metabolic Disease

1. Diabetes mellitus: Definition and Global Burden

Diabetes Mellitus (DM) is a group of disorders rooted in defective glucose metabolism, with manifestations in multiple organ systems involving vascular, endocrine, neurological, and inflammatory consequences (1). The multifacted nature of diabetes complications and the dramatic increase in its global prevalence from 108 million cases in 1980 to more than 500 million in 2018 situates the disease as a frontrunner in morbidity and mortality, ranking 7th in the World Health Organization's list of global causes of death in 2016 (2–4). However, coming in at 1st and 2nd place are ischemic heart disease and stroke, two diseases whose risk is drastically increased by DM (4). In fact, adults with diabetes generally have a 50% higher risk of death from any cause than those without (5). Moreover, the situation is not expected to improve, with projections anticipating a 54% increase in the prevalence of DM by 2030 in the US alone, partly due to an aging population, an increase in obesity, and the adoption of a sedentary lifestyle that facilitates its development (5,6). The surge in DM is expected to be even greater in middle- and lower-income countries, where diabetes is affecting an increasing number of young individuals in their productive years (3,7). Efforts to curtail this surge have mainly occurred at the level of spreading public awareness of the disease, its complications, and the importance of monitoring blood glucose levels in high-risk individuals. Medical advancements in the management of DM have led to an increase in the likelihood of attaining glycemic control and maintaining blood pressure

and lipid profiles within acceptable ranges, which in turn has led to a decrease in the incidence of end-stage complications of diabetes (8). However, DM management is not only financially costly, but also taxes patient quality of life, and this is compounded when DM is associated with vascular complications, which tend to develop early on in the disease (9−11). In fact, the main cause of death in T2DM is not the hyperglycemia or systemic inflammatory state that accompanies the disease per se. Cardiovascular disease (CVD), including coronary artery, cerebrovascular, and peripheral vascular disease, accounts for two-thirds of mortality among patients with T2DM, who are at a higher risk of not only developing CVD, but of dying of its complications (12,13).

To make matters worse, it has recently been shown that even tight glycemic control had no significant effect on major cardiovascular events or microvascular complications in T2DM (14). The ADVANCE and ACCORD trials, two multinational studies recruiting over 10,000 patients with T2DM and subjecting them to intensive glucose-lowering therapy further verified these findings, suggesting that there is more than hyperglycemia at play in the maintenance and progression of the cardiovascular complications of DM (15,16). Moreover, a significant proportion of type 2 diabetic patients show evidence of advanced microvascular impairment at the time of initial diabetes diagnosis, before overt hyperglycemia (17), which suggests that the cardiovascular manifestations of DM may not be a result of the disease itself, but an independent pathological entity that is propagated by factors other than hyperglycemia. Thus, tackling the cardiovascular complications of the DM pandemic should be approached from a preventative angle that acknowledges the role of early metabolic insults in initiating cadiovascular dysfunction. This necessitates further research to elucidate the mechanisms by which this early dysfunction occurs, if formidable strides

are to be made in decreasing the morbidity and mortality of DM-associated cardiovascular disease.

2. Types of DM

DM is classified into two main types depending on the nature of the primary insult that leads to impaired glucose handling. In type I DM (T1DM), also known as insulin-dependent diabetes, a cell-mediated autoimmune reaction targeting the β-cells of the pancreatic islets and leading to their eventual destruction is triggered by a variety of events, none of which is metabolic in origin (18). Microscopic images taken from T1DM patient pancreatic biopsies around the time of clinical presentation reveal an abundance of immune cells, mainly CD8+ T-lymphocytes, and a large number of apoptotic β-islet cells (19). It is important to note that the rate of β-islet cell destruction in T1DM is variable, with patients experiencing mild hyperglycemia for varying periods of time that can last years before β-cell function decreases to an extent that unmasks the disease (1).

While a chronic immune reaction triggers the development of T1DM, the chronic insult in type 2 DM (T2DM), which accounts for 90-95% of all DM cases, is metabolic in nature, with the central player being resistance to the action of insulin, followed by a decrease in its secretion due to the cumulative effects of glucotoxicity, lipotoxicity, and oxidative stress on β-islet cells, leading to their apoptosis (20).

The main regulator of insulin production is glucose, whose plasma maintenance in the tightly controlled range of 4-6mM is fundamental for the preservation of normal tissue function and the facilitation of growth, development, and repair (21). The rapid increase in plasma glucose that follows food ingestion thus prompts the body to utilize

insulin to increase tissue glucose uptake and decrease glucose-releasing mechanisms including hepatic gluconeogenesis and glycogenolysis. This involves an interplay between three main insulin-responsive tissues: the liver, the skeletal muscle, and adipose tissue, and depends on an intact insulin secretory response by the pancreatic β-islet cells and normal tissue sensitivity to insulin.

T2DM is the end result of a gradual, chronic increase in caloric intake that leads to a myriad of systemic effects, including insulin resistance and dyslipidemia, that occur long before hyperglycemia reaches a clinically diagnosable level (22). In fact, clinical trials involving pharmacotherapy that only mildly reduces hyperglycemia have proven to be beneficial in decreasing adverse cardiovascular outcomes in T2DM patients, by mechanisms speculated to be unrelated to glycemic control. For instance, the LEADER trial that assessed the use of liraglutide, a glucagon-like peptide 1 (GLP-1) analogue, in diabetic patients showed that the rate of occurrence of fatal and non-fatal cardiovascular events was decreased across a follow-up period of 3.8 years in the group receiving treatment (23). In addition, the EMPA-REG trial that tested the effect of SGLT2 inhibitor empagliflozin on cardiovascular outcomes in diabetic patients had similar outcomes that were speculated to be caused by multidimensional mechanisms, including changes in arterial stiffness, cardiac function, cardiac oxygen demand, and cardiorenal effects in addition to a reduction in hyperglycemia (24).

B. Vascular Smooth Muscle Cell Dysfunction in Diabetes

The pathophysiological link between T2DM and CVD is complex and multifactorial, involving an interplay between several factors including hyperglycemia, a systemic proinflammatory state, hypercoagulability, and oxidative stress acting on

multiple levels within and outside of the blood vessel (25). At the level of vascular smooth muscle cells (VSMCs), T2DM induces a change in phenotype (26). VSMCs normally exist in the vasculature in a non-proliferative, contractile state in order to regulate arterial tone. However, unlike their skeletal muscle counterparts, they retain a certain amount of plasticity and are able to convert into a proliferative, synthetic phenotype during injury in order to contribute to the repair process. This phenotypic switch also characterizes cardiovascular dysfunction in certain disease states (27), where increased VSMC proliferation plays a major role in propagating a set of vascular diseases including atherosclerosis, restenosis, and graft vasculopathy. In atherosclerosis, an increase in VSMC proliferative and migratory capacity allows these cells to mediate early atherogenesis by contributing to the formation of a thick fibrous cap that characterizes stable atheromatous plaques. The increase in their secretory capacity also allows these cells to synthesize extracellular matrix which not only contributes to plaque formation but also to the repair of ruptured plaques (28). How and when this switch is activated in various conditions is less clear.

T2DM has been shown to induce a contractile-to-synthetic phenotypic switch that is characterized by a decrease in the expression of α-smooth muscle actin (α-SMA) in favor of the non-contractile, non-muscle β-actin, and the formation of an extensive network of rough endoplasmic reticulum (RER) and Golgi apparatus where there normally is an abundance of smooth endoplasmic reticulum (SER). In fact, the diabetic VSMC undergoes a prominent reorganization of its entire cytoskeleton, not only at the level of actin but also at that of myosin and intermediate filaments (29), resulting in a change in VSMC morphology from spindle-shaped to rhomboid (30).

Mitochondrial dynamics are increasingly being recognized as fundamental to changes in VSMC proliferation in disease states. Formerly thought to be discrete, isolated entities, mitochondria are now viewed as dynamic networks whose morphology is regulated by fusion and fission events, the balance of which is required to maintain mitochondrial stability and function (31). Mitochondrial fission entails the fragmentation of tubular mitochondrial networks into several smaller functioning organelles, and is regulated by the dynamin family of mechanoenzymes, mainly the outer mitochondrial membrane (OMM) proteins, mitochondrial fission 1 (FIS-1) and dynamin-related protein-1 (DRP-1) (32). FIS-1 serves to recruit cytoplasmic DRP-1 to fission foci on the mitochrondrial surface, where the latter assembles its oligomers to form spiral chains around these sites in order to prepare them for fission. Using its GTPase domain, DRP-1 provides the energy for mitochondrial fission through GTP hydrolysis (32). DRP-1 may be regulated at any of the steps required for it to perform its function, from cytoplasmic recruitment to GTPase activity. However, the main mechanism governing the activity of DRP-1 is its phosphorylation at two main C-terminal serine residues, Ser616 and Ser637 (33). Phosphorylation at Ser616 by the pro-mitotic cyclin-dependent kinase Cdk1/cyclinB is the earliest reported mechanism to increase DRP-1 activity (34). However, other kinases have been shown to mediate this function since then (33). The more widely studied regulatory site of DRP-1 is Ser637, which has been an identified target of several kinases including protein kinase A (PKA) and Ca2+/calmodulin-dependent protein kinase Iα (CaMKIα). Phosphorylation at Ser637 promotes a decrease in mitochondrial fission by several mechanisms including a reduction in mitochondrial translocation of DRP-1 and a reduction in GTPase activity (33). Changes in mitochondrial dynamics have proven to be central to the acquisition of

a proliferative phenotype by VSMCs, where a transition from individual, randomly dispersed structures to long filamentous entities marks the entry into a more proliferative state. This transition into the proliferative state was blocked by an inhibitor of mitochondrial fission (35). This provides another mechanism by which VSMC phenotypic switch may mediate a plethora of vascular disorders, as an imbalance in mitochrondrial dynamics may lead to uncontrolled reactive oxygen species (ROS) production, and ultrastructural changes in cellular lipids, proteins, enzymes, and DNA, which form the pathological background for the development of various cardiovascular diseases (36).

C. Diabetes-Induced Cardiovascular Dysfunction: When Does the Clock Start Ticking?

1. Prediabetes: A condition that should not be limited to dysglycemia

a. <u>A Clinical Point of View</u>

Clinically, prediabetes is defined by increased fasting plasma glucose (FPG), impaired glucose tolerance (IGT), and HbA1c levels that are not quite at the level required to diagnose diabetes, but reflect a deteriorating capacity of the body to manage glucose and could eventually progress to diabetes (37). The period of time between prediabetes and diabetes is clinically important, as it is viewed as a chance to counsel patients on their risk of diabetes development and intervene to curb that risk. However, individuals with impaired IGT and impaired fasting glucose are already at higher risk of developing cardiovascular disease, because their underlying pathophysiological disturbances are already expressed, and they frequently manifest all of the same risk factors that place T2DM patients at higher risk of macrovascular complications (38). Moreover, meta-analysis of randomized control trials on prediabetic patients showed

that lifestyle modifications and pharmacotherapy did not result in a decreased risk of cardiovascular death or myocardial infarction across a follow-up period of 3.8 years, indicating that cardioprotective interventions should take place before clinical prediabetes is detected (39). This further suggests that the initiation of cardiovascular dysfuntion accompanying DM may involve mechanisms that are independent of hyperglycemia, and that come into play long before prediabetes can be diagnosed. This has led people to acknowledge that it may be better to define prediabetes in terms of risk of long-term medical outcomes, rather than current dysglycemia (22).

b. Pathophysiology

From the pathophysiological point of view, prediabetes is set into motion by a series of metabolic insults that leads to the propagation of a systemic pro-inflammatory state that eventually acts to desensitize insulin receptors in the liver, pancreas, muscle, and adipose tissue (40). The progression from normoglycemia to dysglycemia is observed when β-cells fail to compensate for insulin resistance by increasing insulin production. Individuals with a robust endogenous insulin response may remain normoglycemic for years despite gaining weight and developing insulin resistance (41). However, this is not to say that they are immune to the cardiovascular risks of prediabetes, despite not fulfilling the criteia for its diagnosis. This may be because normoglycemic individuals that may progress to prediabetes exhibit other defects including increased lipolysis, decreased GLP-1 levels, aberrant pro-inflammatory cytokine expression, and decreased adiponectin levels, that may impact vascular health (42–45). However, due to the multiplicity of factors that are dysregulated en route to dysglycemia, the major cause of dysfunction at the level of VSMCs is poorly defined.

This is further complicated by the fact that the timeline of CVD in diabetes is not well studied, and many of the predisposing factors for prediabetes and diabetes, including obesity and dyslipidemia, are also independent risk factors for cardiovascular disease (46).

2. *Adipose Tissue as an Early Transducer of Metabolic Challenge to Insulin Resistance*

The notion that adiposity increases the risk of mortality dates back to 400 B.C., when the Greek physician Hippocrates noted that "sudden death is more common in those who are naturally fat than in the lean." How an abundance of adipose tissue can lead to an increase in mortality has been a subject of much study. Epidemiologically, obesity has been associated with insulin resistance and type 2 diabetes (47). However, evidence is suggesting that the link between obesity and its comorbidities is not merely correlation, and that there are mechanisms by which an excess of adipose tissue can mediate insulin resistance, cardiovascular disease, and other disorders, thus increasing mortality.

a. Structure and Function of Adipose Tissue

Adipose tissue is a type of connective tissue composed of adipocytes, immune cells, and fibroblasts enmeshed in a thin layer of reticular fibers (type III collagen) and supplied by blood capillaries and sympathetic nerve fibers. Some groups have demonstrated that parasympathetic nerve fibers also innervate adipose tissue, but whether this holds true is controversial (48,49). Although individual or groups of adipocytes may be found throughout loose connective tissue, the fundamental property of adipose tissue is that adipocytes constitute the majority of its cells. Adipose tissue

comes in different types defined by the type of adipocytes present. There are two main types of adipocytes that differ in morphology and function, namely white and brown. White adipocytes are characterized by a single, large lipid droplet that occupies the majority of the cell and is surrounded by a thin strand of cytoplasm containing an eccentric nucleus and a few filamentous mitochondria. Brown adipocytes, however, are multilocular and contain a much larger number of mitochondria that give brown adipose tissue its color. White adipose tissue (WAT) plays a role in energy storage, insulation, cushioning, and hormone production, while brown adipose tissue (BAT) is much more metabolically active, and functions to produce heat by non-shivering thermogenesis through the utilization of uncoupling protein-1 (UCP-1), a transporter that is present in the inner mitochondrial membrane of brown adipocytes. UCP-1 fulfills its role of heat production by dissipating the proton gradient established by complexes of the electron transport chain (ETC), thus releasing energy that is normally destined to be stored as ATP, as heat. This effectively uncouples the ETC complexes from ATP synthase, thus giving the protein its name (50). Human subcutaneous and visceral adipose tissue depots consist of mainly WAT, while BAT is present in small depots in the axilla, around the kidney, along the trachea, and between the ribs (51,52). Perivascular adipose tissue (PVAT), which surrounds most blood vessels, is a hybrid of both (53).

As previously mentioned, adipose tissue is composed of many cell types, and immune cells are a particularly active population of cells when it comes to DM pathophysiology. Macrophages are the main type of immune cell occupying adipose tissue, comprising more than half of the immune cell population present in adipose tissue samples from both lean and obese animals. This amounts to 5% of the total number of cells in adipose tissue in lean mice, and over 50% in obese mice (54).

Adipose tissue macrophages (ATMs) are in fact a group of antigenically distinct cells united by the finding that they all express the macrophage protein, F4/80. There are two main groups of ATMs classified according to whether they express the CD11c integrin. CD11c negative cells predominate in adipose tissue from lean animals, and while both CD11c negative and positive macrophages increase in number as obesity progresses, CD11c+ cells end up as the majority in adipose tissue from obese animals (55). CD11c-cells are also called alternatively activated or M2 cells and normally function to maintain adipocyte homeostasis in the steady state. Part of their function involves engulfing dead adipocytes in order to maintain adipocyte turnover. Because adipocytes are larger than macrophages, phagocytosis involves a special mechanism whereby multiple macrophages surround one adipocyte and release their lysosomal enzymes, thus engulfing the cell with an acidic extracellular compartment that leads to the release of its free fatty acids, which are then taken up by the macrophages. This ring of macrophages that surrounds adipocytes appears like a crown in histological sections, and is thus named a crown-like structure. This is similar to the crown-like structures that form in adipose tissue during obesity, except for the fact that in this case, the majority of macrophages involved are of the M1 inflammatory phenotype, the inflammation ensued driving insulin resistance; on the contrary, adipocyte phagocytosis in lean tissue is necessary to maintain homeostasis (56). An increase in the number of crown-like structures in adipose tissue indicates that there is a greater number of necrotized adipocytes and is correlated with obesity and insulin resistance (57). It is worth noting that CD11c is a marker of macrophage polarization in mice, and that the rat markers of polarization include CD86+ for M1 and CD163+ for M2 (58).

b. Adipose tissue transformation From Storing Fat to Causing Disease: Mechanistic insights

The role of WAT in catalyzing the progression from an increase in dietary intake to insulin resistance and diabetic pathology lies in the fact that it serves the important role of storing excess calories as fat, and is thus one of the first tissues to sense and respond to an increase in caloric intake (59). Of course, the liver and skeletal muscle play a role in metabolizing excess glucose by glycogenesis or catabolism, but they lack the capacity to undergo significant changes in tissue structure in order to accommodate extra calories (60). That capacity uniquely characterizes white adipose tissue, and includes hypertrophy of existing adipocytes in order to increase the amount of fat stored per adipocyte, and hyperplasia through the recruitment and differentiation of adipocyte precursor cells. In general, hypertrophy is the less favorable track for adipose tissue expansion because it entails an increase in adipocyte diameter, which decreases the ability of oxygen to diffuse to the region of the cell that is farthest from the vascular supply. Hyperplasia, on the other hand, is associated with an increase in vascularization and the recruitment of stromal cell types that are essential for the maintenance of adipocyte integrity, making it the "healthier" type of expansion (61). Both hypertrophy and hyperplasia normally take place to different extents in obese individuals, and studies have shown that the propensity of an individual's adipose tissue to undergo different extents of hypertrophy or hyperplasia may be a predictive factor as to whether he/she will acquire insulin resistance (62). However, it is important to note that in morbid obesity, angiogenesis is insufficient to keep up with the vascular demand of the ever-growing white adipose tissue, and thus the hypoxia induced by adipocyte hypertrophy is further compounded (63).

The hypoxia accompanying adipose tissue expansion sets into motion a series of events leading to the establishment of a pro-inflammatory state that begins at the level of the adipocyte and eventually spreads to the systemic circulation and from there to the liver, skeletal muscle, and pancreas, and more importantly, to their insulin receptors. This begins by an increase in adipocyte NF-kB expression, which is a direct effect of hypoxia and mediated through an increase in hypoxia-inducible factor 1α (HIF-1α). NF-kB in turn induces the expression of inflammatory cytokines including IL-1β and IL-6 (64). It has been established that IL-1β plays a fundamental role in propagating insulin resistance through direct effects on the insulin signaling pathway, one of which is decreasing the tyrosine kinase activity of the insulin receptor by inducing serine phosphorylation of insulin receptor substrate 1 (IRS1) (64). A spillover from adipose tissue was proposed to be one of the origins of this increased IL-1β (65).

Moreover, this is accompanied by the recruitment of macrophages that are polarized into the M1 phenotype due to an increase in macrophage inflammatory protein 1α (MIP-1α) secretion and monoctye chemoattractant protein (MCP-1) expression, creating a gradual shift from an anti-inflammatory state characterized by an abundance of M2 macrophages to one that is pro-inflammatory (66). M1 macrophage recruitment directly contributes to the accumulation of inflammatory cytokines that eventually spill over to the systemic circulation. TNF-α is one of the main mediators secreted by these cells, which are believed to be the major source of this cytokine in inflamed WAT, rather than adipocytes. M1 macrophages further stimulate adipocytes to upregulate vascular cell adhesion molecule 1 (VCAM1), a protein expressed by adipocytes that directly recruits M1 macrophages by binding to their α-4 integrin, thus triggering a self-sustained inflammatory loop that aggravates insulin resistance (67).

Obesity also leads to a reduction in adiponectin secretion, a beneficial adipokine that normally stimulates macrophage M2 polarization. This may be due to high fat diet-induced degradation of the sirtuin deacetylase SIRT1, which normally induces adiponectin and IL-4 secretion by adipocytes (68,69). M2 macrophages normally suppress TNF-α production by secreting IL-10, which inhibits its transcription. In addition, the increase in very low-density lipoproteins (VLDLs) and free fatty acids (FFAs) that is observed in obesity induces the secretion of pro-inflammatory M1 cytokines, and activates toll-like receptor 4 (TLR4) signaling in murine adipose tissue macrophages, indicative of M1 activation (70–72)

The insulin resistance that is propagated by adipose tissue inflammation, among other factors, in turn leads to an increased demand on the pancreatic β-islet cells to secrete insulin in order to maintain normoglycemia, resulting in hyperinsulinemia. Hyperinsulinemia further impairs insulin sensitivity by contributing to its main instigator, adipose tissue inflammation, as studies have shown that inhibiting insulin action via diazoxide decreases macrophage infiltration into adipose tissue (73).

Although the phenotypic switch from anti-inflammatory M2 to pro-inflammatory M1 macrophages has been accepted as a model of what happens in obesity-induced adipose tissue inflammation, recent studies are suggesting that the story may not be that simple. Since the M1/M2 classification is based on a specific set of pro- and anti-inflammatory markers, Xu et al. assessed whether there was in fact a difference in total pro- and anti-inflammatory markers between M1 and M2 macrophages by conducting whole transcriptome analysis on these groups of cells. The group could not find a prototype inflammatory phenotype that characterizes M1, but instead found a phenotype representing lysosome-dependent lipid metabolism (74). Moreover, using a

proteomics approach, Kratz et al. could not identify typical markers of M1 activation in macrophages from obese humans, but were able to identify proteins that promote lipid metabolism. This could lead to a better understanding of how we view adipose inflammation, leading to better therapeutic strategies to target it (75).

It is worth noting that the systemic inflammation that eventually causes insulin resistance begins at the level of adipose tissue and accumulates until it spills over from there. This is important because tissues in the vicinity of adipose tissue could be affected by diffusion of inflammatory mediators before systemic inflammation ensues, and is the basis of the notion that subcutaneous adipose tissue expansion is less harmful than visceral (76). The same could be said about perivascular adipose tissue (PVAT) in its relation with the vasculature.

c. Perivascular Adipose Tissue: A Critical Mediator of Vascular Health

Perivascular adipose tissue (PVAT) is an adipose depot that is contiguous with the adventitial layer of most blood vessels and plays a role in regulating vascular health. Its close proximity to the vasculature allows it to exert paracrine effects on vascular smooth muscle cells, the influence of which changes with the progression of prediabetes. Like other adipose tissue depots, PVAT plays a fundamental role as an endocrine organ, secreting a myriad of cytokines, chemokines, and hormones that are collectively referred to as adipokines (77).

The effect of PVAT on vascular contractility was first identified by Soltis et al., who showed that aortas with intact periaortic fat displayed a decrease in norepinephrine-induced contractility compared to those in which the PVAT has been removed (78). This anti-contractile effect remained intact when vessels without adipose

tissue were treated with PVAT-conditioned media (79). The name adipocyte derived

relaxing factor (ADRF) was coined for this substance, and subsequent studies

demonstrated that ADRF attenuates the vasoconstrictive response of a variety of agents

(80). Since then, it has been shown that PVAT mediates a myriad of VSMC functions in

addition to contractility, including cell proliferation and migration.

d. <u>The effect of healthy and diseased Perivascular Adipose Tissue on Vascular Smooth
Muscle Cells</u>

PVAT normally secretes a diverse array of mediators that have different, and

frequently opposing, effects on VSMC contractility, proliferation, migration, and

synthetic ability. The effect that PVAT has on these parameters is usually the net result

of an interplay between adipokines that are secreted in altered amounts in different

states of health and disease (81). Shortly after the discovery of ADRF, an adipokine

known as visfatin was identified as the first known growth factor released by PVAT.

Visfatin has a pro-survival effect on VSMCs, endothelial cells, and macrophages, and is

implicated in the development of atherosclerosis by inducing the proliferation of cells

that are required for the formation of a stable atheromatous plaque (82). Its proliferative

effect on VSMCs is mediated by activation of the ERK1/2 and p38 MAPK pathway

(83). Interestingly, visfatin levels were shown to be higher in PVAT than in

subcutaneous and visceral adipose tissue (77).

Leptin is another major adipokine that mediates a direct vasodilatory effect on

blood vessels. However, its effect on VSMC phenotype is obscure, with some studies

showing that it has a pro-proliferative and migratory effect, while others demonstrating

the opposite. The differential effect of leptin on VSMCs is thought to be propagated by

differences in disease states or species, as studies on rat aortic VSMCs have shown that

leptin plays a proliferative role via upregulation of cyclin D1, ERK 1/2, and NFkB (84,85). This is while human carotid VSMCs from patients with atherosclerosis were demonstrated to undergo decreased proliferation and a downregulation of the leptin receptor upon exposure to leptin (86).

Adiponectin is an adipocyte-specific cytokine whose secretion by PVAT is responsible for protection against the neointimal hyperplasia that follows vascular injury (87). This is because adiponectin is a potent inhibitor of VSMC proliferation, and its marked decrease in obesity contributes to the proliferative phenotype acquired by VSMCs during this state (88). Adiponectin secretion is markedly decreased during obesity, further amplifying the proliferative phenotype characteristic of that state. In addition, adiponectin has a direct vasodilatory effect on blood vessels and participates in the anticontractile role known to be played by PVAT (89).

There is a long list of other adipokines and mediators secreted by PVAT that modulate vascular phenotype and contractility, including resistin, nesfatin, 24drenomedullin, vaspin, omentin, etc. whose levels are affected by various disease states and mediate various others. Moreover, PVAT normally releases a variety of cytokines, including interleukins and TGF-β that play a role in maintaining VSMC health. These mediators are normally released by resident macrophages in PVAT, but their specific role in mediating the phenotypic switch from contractile to synthetic is less well known (77).

The modulation of various adipokines by obesity and metabolic challenge is not exclusive to PVAT and has been demonstrated in subcutaneous and visceral adipose tissue as well. However, perhaps due to its vital role in mediating vessel health, and its

hybrid nature as a both brown and white, or brite, PVAT has one additional mechanism by which it may respond to metabolic challenge: browning (90).

e. PVAT browning: Introducing the beige adipocyte

As previously mentioned, there are two main types of adipocytes: white, which is energy-storing, and brown, which is heat-generating. However, the demarcation between these two types is more fluid in the case of adipose tissues that can undergo browning, or a conversion of white adipocytes into "beige" adipocytes, that resemble brown adipocytes in the multilocular morphology of their lipid droplets and the abundance of their UCP1-containing mitochondria (58). The similarities between brown and beige adipocytes extend to their transcriptional profile, where beige adipocytes have been shown to express genes that are known to be BAT-exclusive, including *Cidea*, *Acrp30*, and *Pparγ2* (59). However, white and beige adipocytes have been shown to be derived from a distinct cell lineage from brown adipocytes, with the formers' precursor being Pdgfr-α+. Moreover, studies have shown that SM22α, a marker of early smooth muscle cell development, is either required to be transiently expressed in beige adipocyte precursor cells, or beige adipocytes and smooth muscle cells share a common precursor. This is distinct from brown adipocytes, which share a lineage with skeletal muscle cells (60).

Not much is known about the response of perivascular adipose tissue to metabolic stress in terms of browning, other than the fact that it has been shown to be favorable in certain disease conditions including hypertension, possibly by alleviating the metabolic stress on white adipocytes and thus decreasing their need to expand to accommodate extra calories (91). This may play a role in preventing the hypoxia and

inflammation related to adipose tissue expansion, but no studies up to date have displayed this phenomenon in action in a model of high fat diet-fed rats.

D. Metformin and Pioglitazone Pharmacotherapy Attenuates Cardiovascular Dysfunction in Prediabetic Patients

Recent studies have demonstrated that pharmacological interventions in patients who are at risk for the development of diabetes but are not dysglycemic resulted in a lower rate of CVD. In the Diabetes Prevention Program (DPP), metformin was shown to be beneficial in reducing the microvascular complications of diabetes across a period of 15 years (92). Moreover, the recent MET-REMODEL trial showed that non-dysglycemic left ventricular hypertrophy patients with insulin resistance displayed improved cardiac function upon treatment with metformin (93). Pioglitazone administered to hyperinsulinemic patients with previous cardiovascular incidents reduced their risk of subsequent stroke or myocardial infarction (94). These effects are in isolation of the role of these two drugs in reducing hyperglycemia, as the patient population that these studies were conducted on has not reached the dysglycemic stage yet. Seeing as metformin and pioglitazone were previously shown to reverse adipose inflammation (95,96), it may be possible to speculate that their role in decreasing PVAT inflammation may be responsible for their effects on cardiovascular function, suggesting an early role for PVAT inflammation in mediating CVD.

CHAPTER II

HYPOTHESIS AND AIMS OF THE STUDY

It is likely that diabetic vascular complications are initiated by factors independent of dysglycemia early on in the timeline of diabetes pathology. However, mechanistic insights into the instigators of this cardiovascular dysfunction have been limited, and there is a lack of studies that characterize CVD in the pre-dysglycemia stage..

Evidence of local adipose tissue inflammation in this stage of metabolic dysfunction prompted us to question the role of PVAT inflammation in early CVD. We hypothesize that early CVD in metabolically-challenged rats is a byproduct of paracrine signaling pathways from neighboring PVAT, that occur before the metabolic and inflammatory markers of DM become systemically detectable.

Our specific aims are:

1. Identify inflammatory and morphological changes in PVAT during early metabolic challenge.

2. Examine whether this is paralleled by changes in aortic contractility in metabolically-challenged rats.

3. Investigate alterations in aortic VSMC phenotype, including proliferation, migration, and the expression of contractile markers, from metabolically-challenged rats.

4. Identify whether metabolically-challenged adipocytes can mediate a VSMC phenotypic switch, via an in vitro model of metabolic challenge.

5. Identify paracrine mediators that may be involved in the PVAT-VSMC

   signaling axis in our model of early metabolic challenge.

CHAPTER III

METHODS

A. Rat Model

1. Ethical Approval

All animal experiments were conducted in accordance with an experimental protocol approved by the Institutional Animal Care and Use Committee (IACUC) and in compliance with the Guide for Care and Use of Laboratory Animals of the Institute for Laboratory Animal Research of the National Academy of Sciences, USA.

2. Experimental Design

Male Sprague-Dawley rats weighing 150 g were randomly divided into four groups at 5-6 weeks of age:

- Control rats fed a normal chow diet of 3 Cal(kcal)/g nutritional value

- HC rats fed a hypercaloric diet of 4.035 Cal(kcal)/g nutritional value

- HC rats fed a hypercaloric diet and treated with 30 mg/kg metformin (Met) twice daily starting week 10

- HC rats fed a hypercaloric diet and treated with 2.5 mg/kg pioglitazone (Pio) once daily starting week 10

Rats were kept at an ambient temperature and humidity-controlled room, in a 12-hour light/dark cycle. All rats had free access to food and water throughout the 12-

week period. Body weight was measured weekly, and caloric intake was calculated daily based on the amount of food consumed. Met and Pio treatment was prepared through levigation with 25g HC diet, and the drug-containing food pellet was administered to different groups as planned.

3. Food Preparation and Macronutrient Composition

Normal chow diet (ENVIGO) was obtained from Teklad Rodent Diets (Madison, WI). The nutritional components of this diet are as follows: 3 Cal/g are distributed such that 54% of caloric intake is from carbohydrates, 32% from protein, and 14% from fat (0.9% saturated fat by weight). The HC diet was prepared in-house and consists of food grade fructose (20% by weight, Santiveri foods, Spain) and hydrogenated vegetable oil (Mazola, 15% by weight, BFSA) added to the normal chow diet. Major electrolytes and vitamins were supplemented to match the concentration in ENVIGO diet and as recommended by the American Institute of Nutrition (97). The final composition of the MHC diet by weight (caloric content) is 18.06% fat (38.68%, 5% saturated fat by weight), 15.8% protein (15.66%) and 46.13% carbohydrates (45.73%). Feeding duration was 12 weeks.

4. Oral Glucose Tolerance Test

At the end of week 12 of HC feeding, rats were fasted overnight, and then challenged using a 2g/kg, 20% glucose solution administered by oral gavage. They were gently restrained, and blood glucose was measured at 0, 15, 30, 60, and 120 minutes after glucose load. A tail vein prick was used to collect blood which was then used to measure glucose via an Accu-Chek Performa glucometer.

5. Blood Chemistry

Blood samples were collected from all rats by retro-orbital bleeding every 4 weeks in order to measure lipid profile and random and fasting blood glucose levels. Samples were centrifuged at 4000 rpm for 10 minutes, and the supernatant serum was stored at -80ºC until the time of analysis. Rats were fasted for 6-8 hours for fasting blood sugar measurements while 12 hours of fasting were required for lipid profile. Fasting was carried out in special fasting cages with free access to drinking water.

6. Determining Serum Levels of Insulin, IL-1β and TGF-β1 via ELISA

Measurement of rat insulin, IL-1β, and TGF-β1 in serum was carried out according to the manufacturer's protocol. ELISA kits were obtained from Bender Medsystems (TGF-β1, Vienna, Austria) and Thermo-Fisher Scientific (IL-1β and insulin, Waltham, MA). In summary, all reagents, samples, and standards were prepared. Then, 100μL standard and sample were added to wells. Plates were covered and incubated at room temperature (RT) for 2.5 hours. After that, the plate was washed 4 times. Following this, 100 μl of biotinylated antibody was added to wells and plate was incubated for 1 hour at RT. After washing the plate, 100 μl of Streptavidin-HRP Reagent was added to each well, and the plate was incubated for 45 minutes. After washing the plate, 100 μl TMB substrate was added to each well, and the plate was left to develop in the dark at RT for 30 minutes. Finally, 50 μl of stop solution was added to each well, and absorbance was measured to calculate the results acquired.

7. Invasive Hemodynamics

Systolic and diastolic blood pressure were measured at week 12.

Rats were anesthetized using 100mg/kg phenobarbital (AUBMC pharmacy). Tracheostomy was performed and the right carotid artery was isolated, cannulated and connected to a Millar transducer to measure mean arterial pressure (MAP). After this, the left jugular vein was isolated, cannulated and connected to a shunt to deliver drugs. After the surgery, the recording was allowed to stabilize for 30 minutes. Increasing doses of phenylephrine were administered (0.25, 0.5, 0.75, 1, and 2 µg) and the change in MAP was recorded.

8. Magnetic Resonance Imaging (MRI) to determine Fat to Lean Ratio

The LF10 minispec nuclear magnetic resonance (NMR) machine (Bruker, MA, USA) was used to measure rat fat to lean ratio using NMR to detect different tissue densities. The values obtained from each rat are compared to a standardized, calibrated rat.

9. Sacrifice and Tissue Collection

At the end of twelve weeks of feeding, rats were sacrificed by decapitation and exsanguination under thiopental anesthesia. A medial incision was used to expose the thoracic cavity. Thoracic aortas were dissected immediately and kept in ice-cold Krebs' buffer continuously aerated with carbogen (95% O_2 and 5% CO_2) for myobath experiments.

Some aorta samples were flash frozen using liquid nitrogen and then stored at -80ºC for the purpose of future molecular work. Some samples were preserved in 4% formaldehyde and stored at RT for imaging purposes. Perivascular adipose tissue surrounding the thoracic aorta was carefully separated, weighed, flash frozen using

liquid nitrogen and then stored at -80ºC for the purpose of future molecular work. Some samples were preserved in 4% formaldehyde and stored at RT for imaging purposes. Retroperitoneal and Epididymal fat pads were collected and carefully dissected, weighed, flash frozen using liquid nitrogen and then stored at -80ºC for the purpose of future molecular work. Some samples were preserved in 4% formaldehyde and stored at RT for imaging purposes.

10. In vitro aortic vessel reactivity

Thoracic aortas from all groups were trimmed free of connective tissue and cut into ring segments of 3 mm length taking into account not to damage the endothelium. Some of the rings were denuded of endothelium mechanically by gently rubbing the intimal surface with a fine steel rod. Aortic rings with and without endothelium were mounted in 12 ml organ baths containing Krebs buffer at 37°C. The pH of the Krebs buffer was maintained at 7.4 by continuous aeration of organ bath with carbogen. In each bath, two stainless steel wire hooks were inserted through the lumen; one was anchored to a stationary support (a metal hook in the organ bath) and the other connected to a force displacement transducer for recording aortic contraction using Labchart pro 8 (Powerlab, AD instruments, Australia). The rings were allowed to equilibrate for 45 minutes under an initial resting tension of 1 g before performing experiments. After 45 minutes of equilibration, 60 mM KCl was added to assess the aortic depolarization and left in contact for 10 minutes before rinsing with Krebs' buffer. Then a range of PE concentrations (10-13- 3x10-4 M) in half-log increments were used in a cumulative fashion to establish the concentration-response curve and investigate the contractile changes occurring to the aortic rings from the different

groups. The contractile response at each concentration was normalized to the maximum tension obtained. The normalized values were used to plot the Log [PE] vs. response curve. Log EC50 values were obtained by fitting the results of six replicates in each group using GraphPad Prism software (GraphPad Software, California, USA).

11. Immunohistochemistry and Imaging

For histopathology and immunohistochemistry, formalin-fixed aortas were embedded in paraffin, sectioned transversely, and placed on clean slides. Staining was performed simultaneously for accurate comparison. For demonstration of nucleus and cytoplasmic inclusions, hematoxylin and eosin staining was used, while for estimation of reactive oxygen species activity dihydroethidium (DHE) staining was performed on cryosectioned aortas. Briefly, cryosections were air dried. DHE stain was added to the tissue at a final concentration of 15 μM. Slides were kept in a light-proof container and incubated at 37°C for 45 min. Fluorescent images were obtained through Alexa Fluor 568 filter for the DHE red fluorescence that was measured against the green collagen autofluorescence obtained through the Alexa Fluor 488 filter. Immunohistochemistry was done for detection of TGF-β and Smad3 in aortas and CD68 in perivascular adipose tissue and aortas. Sections were incubated with 1:100 dilution of primary antibody (rabbit anti-TGFβ, rabbit anti-Smad3, and rabbit anti-CD68, Abcam, Cambridge, UK) and detected using Novolink Polymer Detection Kit (Leica Biosystems, Buffalo Grove, IL) according to the manufacturer's protocol. Medial thickness was determined in aortic sections stained with hematoxylin and eosin. Sections were deparaffinized and hydrated with deionized water. Slides were stained in hematoxylin solution for 90 seconds then

rinsed in running tap water. Finally, sections were dehydrated, cleared and mounted in toluene or xylene based mounting media.

12. Oil-Red-O Staining

Stock solution was prepared by dissolving 500mg of Oil-O-Red powder in 100mL isopropanol using gentle stirring and heating. Working solution was prepared by adding 6 volumes of stock solution to 4 volumes double distilled water (ddH_2O), and filtered before use.

Frozen PVAT that was stored at -80ºC was sectioned into thin laminae and hydrated. It was then incubated in 5% formalin for 1 hour, washed twice with ddH_2O, and then twice with 60% isopropanol. Working solution of Oil-O-Red was then added to the tissue and incubated for 15 minutes. Next, 2 washes with 60% isopropanol were carried out followed by 2 washes with ddH_2O. The samples were then imaged using a Leica light microscope.

13. Western Blot

Tissue samples kept at -80ºC were crushed under liquid nitrogen. 10 mg of tissue was transferred to 1 ml of protein extraction buffer containing 1% sodium dodecylsulfate (SDS), 0.9% NaCl, 80 mM Tris hydrochloride (pH 6.8), and 100 mM dithiothreitol. Tissue amounts used for protein extraction were optimized with respect to final protein concentration in preliminary experiments. Samples were heated for 10 min at 95°C, allowed to cool down and transferred to a rocking shaker and left overnight for protein extraction at 4°C. In case of cell samples, cells were obtained by washing with 1x phosphate buffered solution (PBS) (Sigma-Aldrich) and scraping with cell scrapers.

Afterwards, they were centrifuged to obtain a pellet that was transferred to the extraction buffer detailed above. Aliquots with equal protein content from the extracts were then used for SDS-PAGE and blotting. After transfer and fixation, nitrocellulose membranes were blocked with 5% skimmed milk (Bio-Rad, Hercules, CA, USA) in Tris-buffered saline containing 0.1% Tween 20 (0.1% TBST) for two hours at room temperature. At this stage, membranes were cut at the appropriate molecular weights to allow for probing of multiple proteins within the same run. Membranes were incubated in a dilution of primary antibodies in 1% skimmed milk in 0.1% TBST (1:1000 for rabbit anti-AMPKα, anti-P-AMPKα, anti-P-Erk1/2, anti-P-DRP-1 (Ser616), anti-DRP1, anti-P-DRP1 (Ser637), anti-P-IKK, anti-UCP1 (Cell Signaling, MA, USA), anti-Erk1/2 (ThermoFischer Scientific, MA, USA), anti-NFkB, anti-PPARγ, anti-HIF1α, anti-GAPDH (Abcam) and 1:500 for rabbit anti-IL-1β and TGF-β1 (Abcam)) overnight at 4°C. After washing with 0.05% TBST (4 x 5min), membranes were incubated in 1:10,000 biotin-conjugated goat anti-rabbit Ig for 1 h at room temperature followed by washing and incubation with 1:100,000 horse radish peroxidase-conjugated streptavidin at room temperature for 30 minutes. Following washing 4 x 5 min with 0.05% TBST and 2 x 5 min with TBS, membranes were exposed to Clarity Western ECL substrate (BioRad, Hercules, CA) for 5 min following by image detection using ChemiDoc imaging system (BioRad, Hercules, CA). Band optical density was measured using Image J software and a ratio of arbitrary density units was obtained for the protein band of interest and the density of the band representing the housekeeping gene, GAPDH, after stripping and re-probing, to correct for variabilities in loading and sample concentration.

14. Quantitative Real-Time Polymerase Chain Reaction (Q-PCR)

Total RNA was extracted using RNeasy Mini kit with DNase treatment (Qiagen, Hilden, Germany) and first strand cDNA produced with the Sensiscript RT kit (Qiagen, Hilden, Germany) with oligo d(T) primer. Primer pairs to identify rat IL-1β , TGF-β1 and β-actin were used. Primers were designed using the primer-BLAST tool based on gene sequences from the Nucleotide database available from the National Center of Biotechnology Information in USA. The following primers were ordered from Sigma (St. Louis, Missouri, USA):

IL-1β forward GCCTCAAGGGGAAGAATCTATACC, reverse GGGAACTGTGCAGACTCAAACT; TGF-β forward ATTCCTGGCGTTACCTTGG, reverse AGCCCTGTATTCCGTCTCCT; β-actin forward GTCAGGTCATCACTATCGGCAAT and, reverse AGAGGTCTTTACGGATGTCAACGT. Primer sets had an estimated efficiency of >90% that did not differ by >5% at the annealing temperature and gave a single peak with no evidence of other amplicons or primer dimer synthesis during melt curve analysis. Q-PCR was carried out with SYBR-Green and a reaction that had a hot beginning at 95°C for 5 min, followed by 40 cycles of 95°C for 15 s, 60°C for 1 min and 72°C for 1 min. Threshold cycle was established with a Bio-Rad iCycler (Hercules, CA) and vendor-supplied software, and transcript abundance was computed by the $2^{-\Delta\Delta Ct}$ method with β-actin as the reference for normalization.

B. In Vitro cell work

1. Isolation and Culture of Rat Thoracic Aortic VSMCs

Rat thoracic aortas were isolated and placed in 2mL of serum free Dulbecco's Modified Eagle Medium (DMEM) F12 (Sigma) at 4ºC. The following steps were carried out in a biosafety cabinet under aseptic conditions: the aortic section was cleaned from adventitial tissue using sterile forceps and scissors. It was then cut longitudinally to reveal the endothelial cell layer which was scraped off gently. It was then cut into four pieces and placed in 2mg/mL collagenase IA solution (Sigma) for 45 minutes at 37ºC with gentle shaking. After incubation, aortic segments were isolated and incubated at 37ºC in sterile T-25 flasks (Corning) with 5mL of Complete DMEM F12 (10% Fetal Bovine Serum (FBS), 1% Penicillin-Streptomycin) (Sigma). Flasks were checked daily for cell adherence, which was observed 3-7 days after culture. Once 80% confluent, cells were detached using 1x Trypsin-EDTA solution (Sigma), and sub-cultured. Assays were carried out on cells once passage 3 had been attained.

2. MTT Assay

MTT was obtained from abcam in powdered form and dissolved in 1x phosphate buffered solution (1xPBS) at a concentration of 5mg/mL. Cells were seeded into a sterile 96-well plate (Corning) at a count of 5000/well, and left to attach for 24 hours. After this, treatment was added depending on the experiment at hand. When treatment duration was over, the media in each well was replaced with 100µL of fresh media, to which 20µL MTT solution was added. The plate was then wrapped in aluminum foil and incubated at 37ºC for 3 hours, after which the media/MTT mixture was aspirated and replaced with 100µL of dimethyl sulfoxide (DMSO) and left to incubate for an

additional hour. The plate was read using the Multiskan EX spectrophotometer (ThermoFisher) at 570nm.

3. Cell Migration Assay

Cells were seeded into a six well plate (Corning) at a density of 90,000 cells/well, and left until 90% confluence was attained. Then, a scratch was made in the center of the well using the top of a yellow pipette tip. Images were acquired at this time, designated T=0, at labelled positions on the well lids. After 24 hours, images were taken at the same position and percentage migration was assessed by measuring the distance traversed by the cells using imageJ.

4. Immunofluorescence

Immunofluorescence staining was done by plating sterile coverslips into a 12 well plate (Corning) and seeding 5000 cells/well. Cells were left to attach for 24 hours, after which treatment was added as necessary. Once the time of treatment had elapsed, cells were washed twice with PBS 1X, before removal of coverslips and fixation in 2% formaldehyde for 30 minutes at room temperature. This is followed by two washing steps with PBS 1X, and cell permeabilization using 0.1% Triton X-100 in 1X PBS for 30 minutes at room temperature. Another PBS 1X washing step follows, after which the cells are left in 3% normal goat serum (NGS) for an hour of blocking at RT. The cells are then incubated overnight with primary antibody in 1% NGS at 4ºC. The concentrations of antibody used are 1:100 for rabbit polyclonal α-SMA and 1:50 for rabbit monoclonal Calponin (Both from abcam, MA, USA). The next day, cells are washed thrice with 1X PBS and incubated with fluorescein isothiocyanate (FITC)-

conjugated secondary goat anti-rabbit antibody (abcam) at 1:100 in 1% NGS for 1 hour at RT in the dark. Cells are then washed thrice with 1X PBS, and diluted Hoescht stain (1:10000) is added and left for 5 minutes incubation at RT in the dark. Cells are washed with 1X PBS for one last time and the coverslips are mounted on microscope slides using ProLong© Gold AntiFade Reagent (Thermo Fisher Scientific, MA, USA). Slides are left to dry overnight at 4ºC and imaged the next day using a Zeiss Axio microscope at 495/519nm excitation/emission spectrum for FITC and 358/461nm for Hoescht stain.

5. *Propidium Iodide Staining*

Cells were seeded at a density of 700,000 cells/well in a 6 well plate (Corning). After leaving them to attach overnight, cells were serum starved for 24 hours by replacing their complete media with serum free media. They were then detached, centrifuged at 1200 rotations per minute for 5 minutes, and the supernatant was discarded. Cells were then resuspended in 5mL of pre-cooled 70% ethanol. Cells were then stored overnight at -20ºC. The next day, cells are spun down in the ethanol at 200g for 5 minutes at RT. Ethanol was then aspirated, and the cells were washed with 1XPBS, after which they were centrifuged at 400g for 5 minutes at RT. Cells were then incubated for 45 minutes at 37ºC with ribonuclease (Sigma) at a concentration of 0.2mg/mL, to ensure that only DNA is stained. Then, cells are centrifuged once more at 400g for 5 minutes, resuspended in 1mg/mL propidium iodide staining (ThermoFisher), and incubated at 37ºC for 45 minutes. After this, cells were centrifuged at 400g for 5 minutes and resuspended in 1X cold PBS for sorting using Guava EasyCyte8 Flow Cytometer Millipore.

6. Mitotracker Staining

Mitotracker Orange CMTMRos was obtained from Sigma in powdered form, and reconstituted in DMSO (Sigma) to prepare a 1mM stock solution. Working solution of Mitotracker Orange was prepared fresh at a concentration of 100nM in DMEM F12 serum free media (Sigma). Hoescht Stain obtained from Sigma in ready-to-use Molecular Probes form. Coverslips were placed into a 12 well plate (Corning) and cells were seeded at a density of 5000 cells/well. Cells were left to attach for 24 hours, after which treatment was added as necessary. Once treatment time had elapsed, cells were washed with 1 x PBS (Sigma) and Hoescht stain at a concentration of 2 drops/mL of serum free media was incubated with the cells for 20 minutes at 37ºC. After this, the cells were washed with 1X PBS, and the working solution of Mitotracker Orange was added to each well at a volume of 200µL per well. The plate was left to incubate for 20 minutes at 37ºC while wrapped in aluminum foil, after which the cells were washed with PBS 1X (Sigma), the coverslips removed and adhered to microscopic slides using ProLong© Gold AntiFade Reagent (ThermoFischer). The microscope slides were then placed overnight at 4ºC in the dark before being imaged at an excitation/emission spectrum of 554/576 nm for Mitotracker and 361/497 nm for Hoescht stain.

7. Pre-adipocyte to Adipocyte Differentiation

3T3-L1 cells were seeded into T-25 flasks and left to attach and grow until 70% confluence is attained. At this stage, their media was discarded and replaced with high glucose DMEM (Sigma) induction medium containing 0.1mM 3-isobutyl-1-methyl xanthine (IBMX), 1µM dexamethasone, and 20mIU/L insulin. This was considered day 0 of differentiation. At day 3, induction medium was replaced with medium containing

20mIU/L insulin for an additional 4 days. After the elapsed time, this medium was replaced with complete high glucose DMEM once again.

Bone marrow mesenchymal stem cells (BMMSCs) were seeded into 6 well plates (corning) and cultured until 50% confluence was attained. At this stage, their media was discarded and replaced with DMEM F12 (Sigma) induction medium containing 0.1mM IBMX, 1μM dexamethasone, 40mIU/L insulin, and 2μM pioglitazone. This was considered day 0 of differentiation. At day 5, induction medium was replaced with medium containing 40 mIU/L insulin and 2μM pioglitazone insulin for an additional 5 days. After the elapsed time, this medium was replaced with complete DMEM F12 once again.

8. Adhesion Assay

Adipocytes or VSMCs were seeded into a 96-well plate at a concentration of 5000 cells/well, and were left to attach for 24 hours, after which their medium (DMEM F12 (Sigma)) was replaced with either DMEM F12 containing 1600μM free fatty acids (Sigma) and 40mIU/L insulin or control DMEM F12. After 24 hours, the medium was aspirated, and THP-1 cells labelled with Hoescht Molecular Probes stain (Sigma) were added at a density of 20,000 cells per well into each well. After 30 minutes incubation time at 37ºC, the THP-1 containing medium was aspirated and the wells washed twice with PBS 1X (Sigma). The plate was later taken to be read by the Fluoroskan Ascent FL spectrophotometer (ThermoFisher) at an excitation/emission wavelength of 361/497nm. Images of the cells were later taken using a Zeiss Axio microscope at the same excitation/emission spectra for monocytes, and superimposed on brightfield images in order to visualize the non-labelled cells (adipocytes or VSMCs)

9. Fluorescence-Associated Cell Sorting (FACS)

THP-1 cells were added to pre-treated adipocytes in T-25 flasks at a density of 1,000,000 cells/flask, and left for 24 hours. After this, cells were detached using 1X Trypsin-EDTA and washed using 10% FBS an 1% Sodium Azide (all were obtained from Sigma) in 1X PBS washing buffer. Antibodies were added to the cells at 1:50 dilution in 3% bovine serum albumin (BSA) in 1X PBS. Anti-CD45 and anti-CD86 were obtained from ThermoFisher, and Anti-CD163 from Bioss Antibodies (MA, USA). Isotype controls were used to correct for background staining. After incubation for 30 minutes at 4ºC in the dark, cells were washed 3 times using the washing buffer previously described, and resuspended in 1mL washing buffer to be sorted. Sorting was done using Guava EasyCyte8 Flow Cytometer Millipore.

C. Statistical Analysis

Data were expressed as Mean ± SEM. Comparisons between groups were done using One Way ANOVA followed by Dunnett post-hoc test, or Two Way ANOVA followed by Sidak's multiple comparisons test in comparing different time points or doses among groups. Student's t-test was also used when appropriate. GraphPad Prism software was utilized for analysis. P value < 0.05 was considered statistically significant.

CHAPTER IV

RESULTS

A. Metabolic Consequences of Twelve Weeks of Hypercaloric Feeding

Rats fed an HC diet consumed ~14 calories than their control counterparts per day, and this did not vary across 12 weeks of feeding (Figure 1A). However, the increase in caloric intake did not impact body weight, as 12 week HC-fed rats were of comparable weights to controls (Figure 1B). However, there was a 25% increase in fat: lean ratio in the HC-fed group (Figure 1L).

Glycemic indices including HbA1c, fasting blood glucose, and random blood glucose remained unchanged at 12 weeks of feeding, but began to increase at 16 weeks, indicating that progression to prediabetes and diabetes is expected if this diet is maintained, similar to a high fat diet in humans (Figure 1 C-F). In addition, no changes in diastolic and systolic blood pressure were observed, limiting the insult to hyperinsulinemia and hyperlipidemia (Figure 1 H-K).
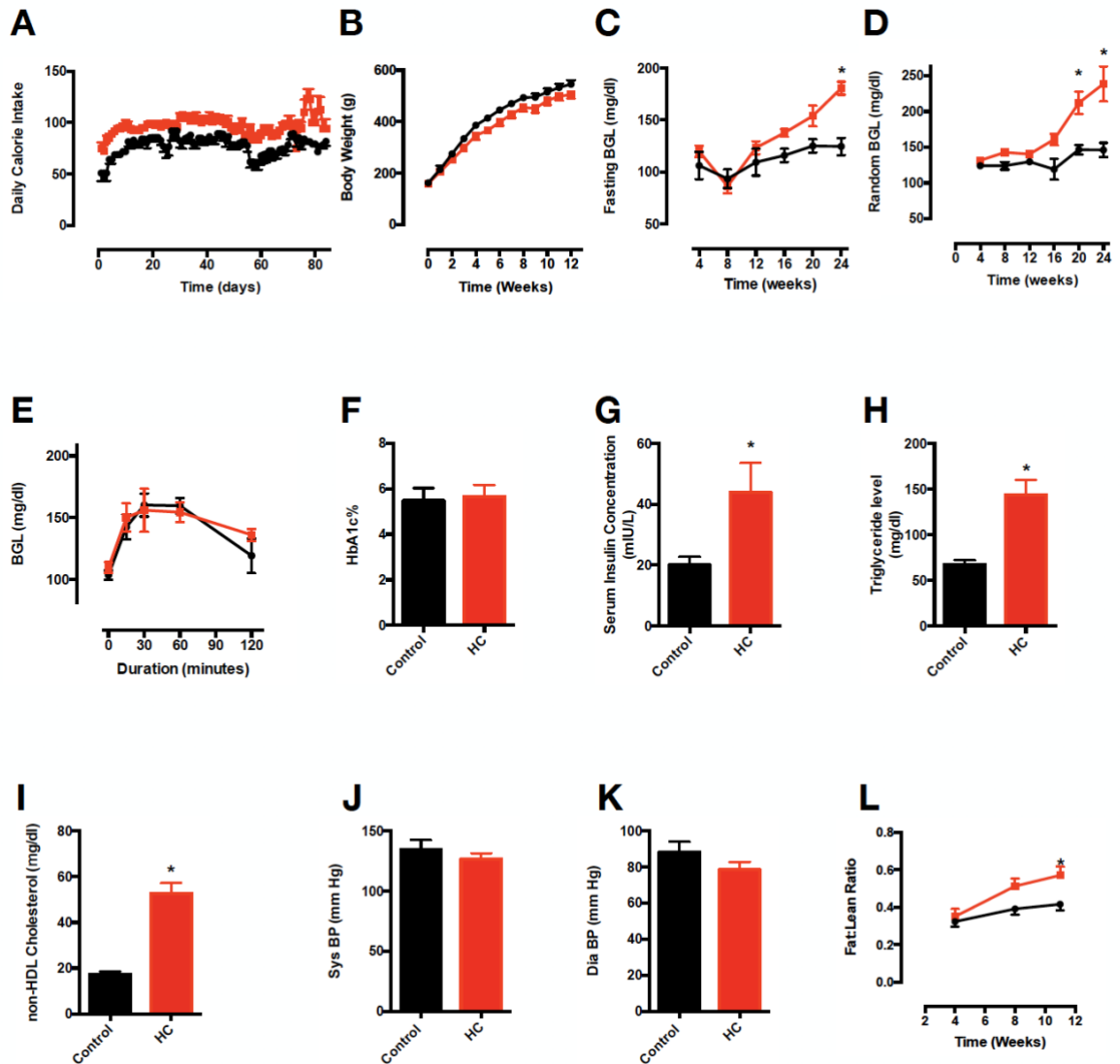
Figure 1. Metabolic Consequences of 12 weeks of Hypercaloric Feeding.

A, Daily caloric intake in HC-rats versus control rats over 12 weeks of feeding (n=8); B, Weight gain in 12 week HC-fed rats versus control (n=8); C, Fasting blood glucose levels in HC and control rats over 24 weeks (n=5); D, Random blood glucose levels in HC-fed and control rats over 24 weeks (n=5); E, Blood glucose levels prior to and at different time intervals after an oral glucose load (n=5); F, HbA1c levels in HC-fed rats versus controls at 12 weeks of feeding (n=5); G, Fasting serum insulin concentration in HC-rats versus controls at 12 weeks of feeding (n=5); H, Triglyceride levels in HC-fed rats versus controls at 12 weeks of feeding (n=5); I, non-HDL cholesterol levels in HC-fed rats versus controls at 12 weeks of feeding (n=5); J, Systolic blood pressure in HC-fed rats versus controls at 12 weeks of feeding (n=5); K, Diastolic blood pressure in HC-fed rats versus controls at 12 weeks of feeding (n=5); L, Fat: lean ratio in HC-fed rats versus control across 12 weeks of feeding (n=5). Statistical analysis was done by two-way

B. Twelve-Week Hypercaloric Feeding Induces Perivascular Adipose Tissue Inflammation Without Causing Systemic Inflammation or Local Inflammation in Other Adipose Tissue Depots

Oil-Red-O staining revealed an increase in lipid droplet size in HC-fed rats that was slightly attenuated by metformin treatment and significantly attenuated by pioglitazone (Figure 2A). This was accompanied by an increase in the hypoxia marker hypoxia-inducible factor 1α (HIF-1α) (Figure 2, D&E) and the pro-inflammatory mediators NF-kB, P-IKK (Figure 2 D-G), IL-1β, and TGF-β1(Figure 3A). In addition, IHC staining for CD68 revealed an increase in crown-like structures in the HC group, which was reversed by treatment with metformin and pioglitazone (Figure 2A). An upregulation in p38 MAPK was also observed in the HC-group, but this was not attenuated by metformin and pioglitazone (Figure 2 F&G).HC-fed groups exhibited an increase in UCP-1, which was reversed beyond initial levels by metformin and pioglitazone (Figure 2 F&G). The opposite was observed with PPAR-γ, where HC-fed rats showed a decrease in levels of this transcription factor, and these is was unchanged in the metformin and pioglitazone treated groups (Figure 2 D & E). Interestingly, the increase in IL-1β and TGF-β1 mRNA levels was not observed in retroperitoneal and epididymal adipose tissue (AT), limiting this pro-inflammatory change to PVAT (Figure 3 A&B). This is despite an HC-induced increase in weight of epididymal AT, and a lack of change in PVAT weight (Figure 3D). Serum IL-1β and TGF-β1 also remained the same, indicating that inflammation had not attained a systemic level (Figure 3C).
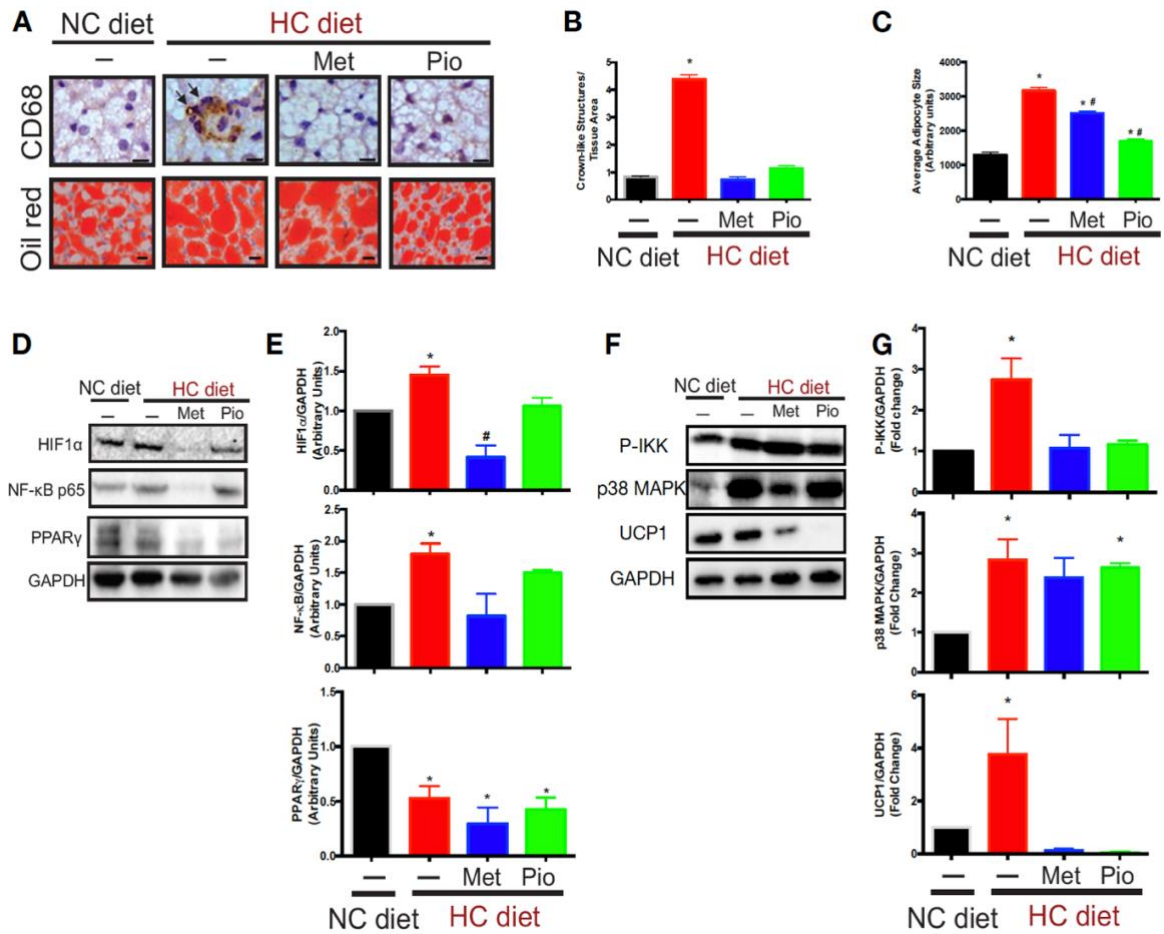
Figure 2. Changes in Perivascular Adipose Tissue Structure and Inflammatory Profile at 12 weeks of HC Feeding.

A, Top panel: Images from CD68 immunohistochemistry staining on PVAT. Crown-like structures in the HC panel are indicated by arrows. Bottom panel: Images from Oil-O-Red staining. Scale bars are 10μM; B, Quantified number of crown-like structures observed on IHC staining in A (mean crown-like structures/tissue area ± SEM, n=3); C, Quantified lipid droplet size observed on Oil-O-Red staining in A (mean adipocyte size ± SEM, n=3); D, Representative blots of HIF-1α, NF-kB, and PPARγ; E, Quantified protein levels of HIF-1α, NF-kB, and PPARγ (mean optical density ± SEM, n=3); F, Representative blots of P-IKKβ, p38 MAPK and UCP1; G, Quantified protein levels of P-IKKβ, p38 MAPK, and UCP1 (mean optical density ± SEM, n=3). Statistical analysis was done by one-way ANOVA followed by Tukey multiple comparisons test. * denotes $P < 0.05$ vs. control rats, while # denotes $P < 0.05$ vs. HC-fed rats.
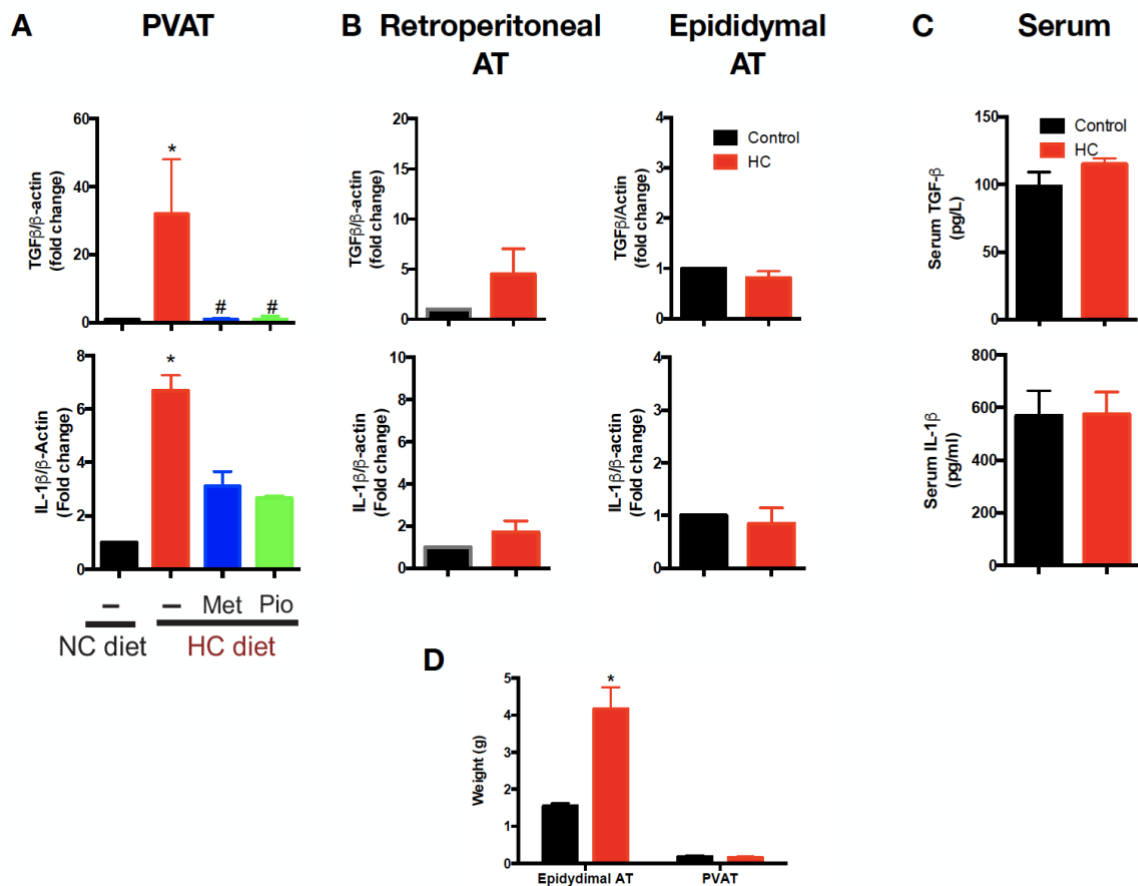
Figure 3. PVAT inflammation as compared to other adipose tissue depots and systemic circulation.

A, IL-1β and TGF-β1 mRNA expression profiles in PVAT of 12 week HC-fed rats compared to control, metformin, and pioglitazone treated rats; B, Retroperitoneal and epididymal adipose tissue IL-1β and TGF-β1 mRNA expression in12 week HC-fed rats compared to control, metformin, and pioglitazone treated rats; C, Serum levels of IL-1β and TGF-β1 in control and HC-fed rats; D, Weight of epididymal AT and PVAT in HC-fed rats compared to controls at 12 weeks of feeding. For A-C, statistical analysis was done by one-way ANOVA followed by Tukey multiple comparisons test. For D, statistical analysis was done by unpaired t-test. * denotes $P < 0.05$ vs. control rats, while # denotes $P < 0.05$ vs. HC-fed rats.

C. Twelve-Week Hypercaloric Feeding Induces Aortic Inflammation that is Reversed by Metformin and Pioglitazone Treatment

At the level of the thoracic aorta, 12-week HC feeding induced inflammation

that is mediated by TGF-β1 and IL-1β, as shown using immunohistochemistry (IHC)

and western blot, respectively (Figure 4A). In addition, Smad3, one of the main

transducers of the TGF-β1 signaling pathway, was also increased (Figure 4A).

However, the surge in inflammatory mediators was not coupled with macrophage

recruitment, as evidenced by the lack of increase in CD68 staining on IHC (Figure 4A),

indicating that inflammation is still in its early stages. This was coupled by an increase

in reactive oxygen species (Figure 4A), which is known to be elevated during

inflammation and is a hallmark of cardiovascular disease (98).

Increased phosphorylation of ERK1/2 was observed upon hypercaloric feeding

(Figure 4B), which is not surprising given that ERK1/2 activation is downstream of

both TGF-β1 and IL-1β, and has been shown to trigger vascular remodeling (99), which

was observed as thickening of the vascular smooth muscle layer on H&E (Figure 4A).

In addition, a decrease in P-AMPK was observed, which was ameliorated by metformin

and pioglitazone (Figure 4B). In fact, metformin and pioglitazone ameliorated much of

the inflammatory changes observed in HC feeding (Figure 4), which supports their

proven efficacy at improving cardiovascular dysfunction in prediabetes (92,94).
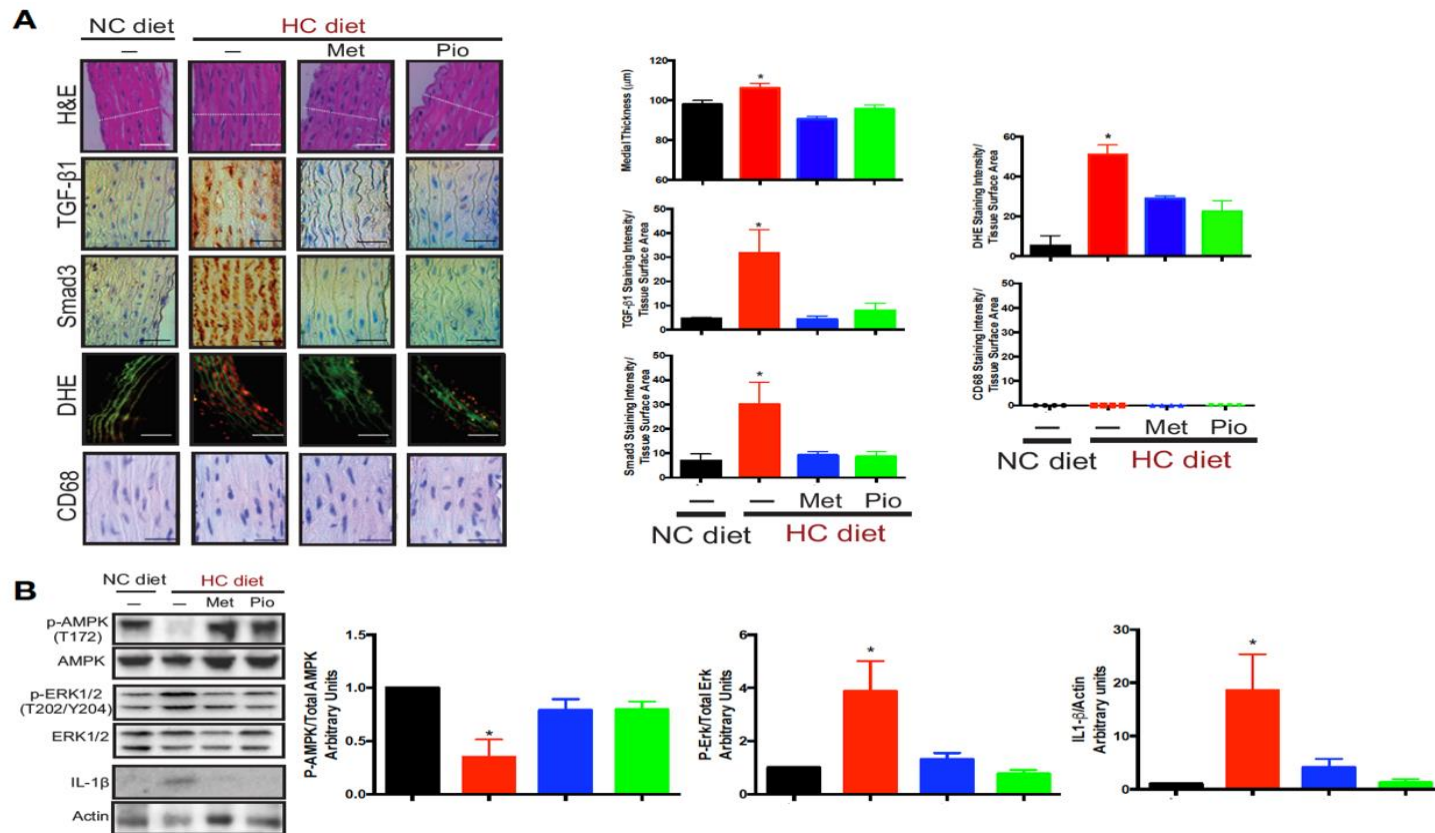
Figure 4. Structural and Inflammatory Changes in the Thoracic Aorta Are Mediated by a Hypercaloric Diet.
A, Representative images of various staining techniques done on thoracic aortas of 12-week control, HC, metformin, and pioglitazone rats Panel 1 (top): H&E. Panel 2: IHC TGF-β1 Panel 3: IHC Smad3. Panel 4: DHE. Panel 5: IHC CD68. Immunohistochemical staining is shown in brown on a counter stain of H&E, while DHE is shown on the counter green autofluorescence of collagen. Scale bars are 40μm for H&E and immunohistochemistry, and 80μm for DHE staining (n=4); Right, Quantification of the images represented on the left panel (mean medial thickness ± SEM for H&E, mean staining intensity per tissue surface area ± SEM for IHC, and DHE, n=4); B, Representative western blots for P-AMPK, AMPK, P-ERK1/2, ERK1/2, and IL-1β on 12 week control, HC, metformin and pioglitazone rats (left), and quantified results (mean optical density ± SEM, n=3). Statistical analysis was done by one-way ANOVA followed by Tukey multiple comparisons test. * denotes P < 0.05 vs. control rats, while # denotes P < 0.05 vs. HC-fed rats.

D. Twelve-Week Hypercaloric Feeding Induces Thoracic Aortic Hypercontractility

Metabolic challenge-induced aortic changes were not limited to the structural and inflammatory level. Aortic dysfunction in the form of hypercontractility was observed in the thoracic aorta in multiple experiments. Firstly, thoracic aortic rings exhibited increased contraction in myobath experiments (Figure 5B). In addition, maximal contraction upon exposure to the pro-contractile agent, phenylephrine, was increased in aortas from HC rats (Figure 5A). Mean arterial pressure was also found to be increased in HC aortas (Figure 5C). The increased contractility was partially ameliorated by metformin and pioglitazone treatment, which indicates that their benefits are not limited to the anti-inflammatory and structural (Figure 5 D-F).
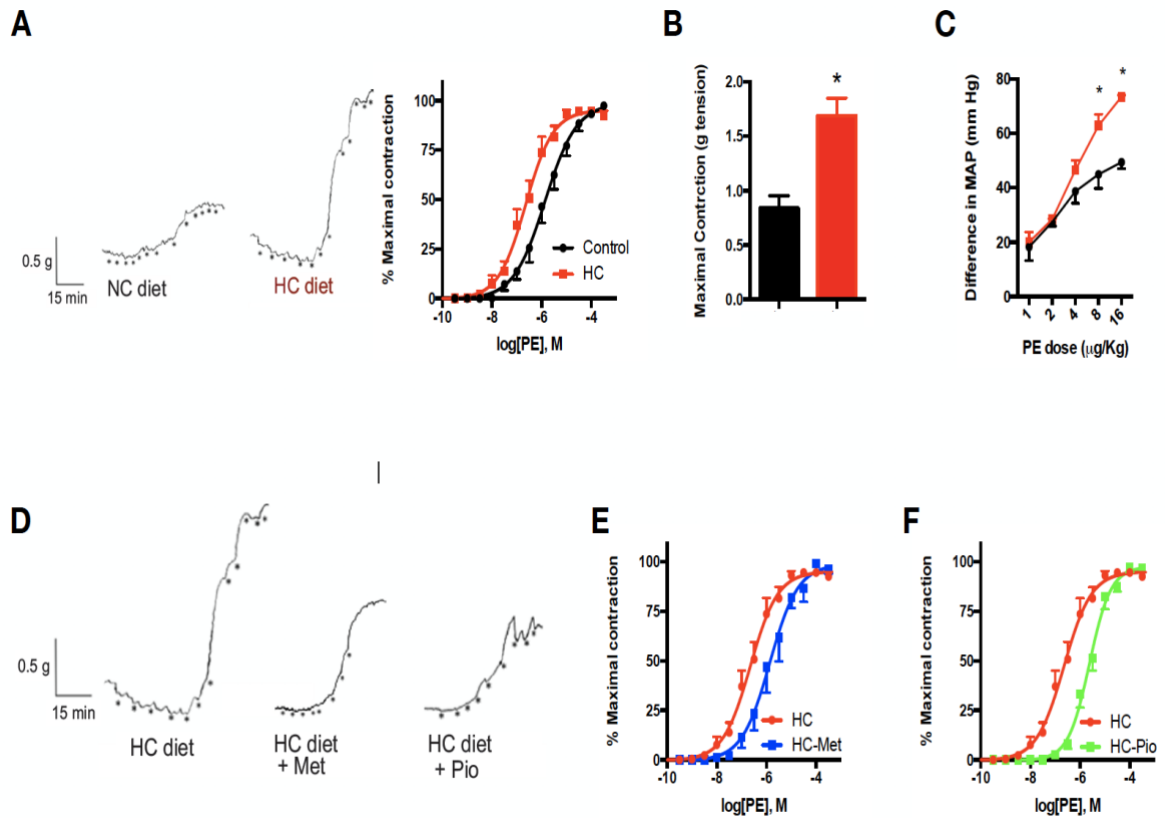
Figure 5. Twelve Week Hypercaloric Feeding Induces Aortic Hypercontractility.
A, Representative tracings (left) and maximal contraction of aortic rings (right) from control and HC-fed rats in response to phenylephrine (n=8); B, Maximal aortic contraction in 12 week control and HC-fed groups (n=8); C, Mean arterial pressure (MAP) as a function of phenylephrine dose in 12 week HC-fed and control rats (n=8); D, Representative tracings of aortic rings from 12 week HC-fed, metformin and pioglitazone rats (n=8); E, Maximal aortic contraction as a function of phenylephrine dose in 12 week HC-fed and metformin rats (n=8); F, Maximal aortic contraction as a function of phenylephrine dose in 12 week HC-fed and pioglitazone rats (n=8). Statistical analysis was done by one-way ANOVA followed by Tukey's multiple comparisons test. * denotes $P < 0.05$ vs. control rats.

E. VSMCs isolated from rats fed an HC-diet exhibit changes suggestive of a contractile-to-synthetic phenotypic switch

VSMCs isolated from HC-rats exhibit a decrease in the contractile markers, α-smooth muscle actin and calponin, upon immunofluorescence staining (Figure 6 B, C).

When coupled with the increase in migration that was also observed (Figure 6D), these findings suggest that a phenotypic switch from contractile to proliferative is occurring.

A decrease in metabolic activity was observed on MTT assay in HC cells (Figure 7A), which could indicate that cell proliferation is decreasing. However, this was shown to be unlikely given the results of cell cycle analysis (Figure 7B), which showed that there is no significant difference in the number of cells in each stage of the cell cycle between control and HC groups. Furthermore, western blots that demonstrated an increase in DRP-1 phosphorylation at Ser616 (Figure 7C) suggest that mitochondrial dysfunction may be responsible for the results of the MTT assay. Although an increase in DRP-1 phosphorylation at Ser637 was observed (Figure 7D), which promotes mitochondrial fusion, the change is smaller than that of Ser616, so it is likely that mitochondrial fission is the predominating event. Mitotracker staining supported these results (Figure 7E), as the formation of mitochondrial networks was noted in control VSMCs, while the mitochondrial distribution of VSMCs from HC-fed rats was more diffuse. Moreover, mitochondria from HC-fed rats stained less intensely, which means that they are functioning at a lower capacity, because mitotracker staining is dependent on membrane potential.

Metformin and pioglitazone treatment ameliorated the decrease in contractile markers (Figure 6 B and C), but exhibited a surprising increase in migration beyond what is observed in the HC-fed rat VSMCs (Figure 6D).
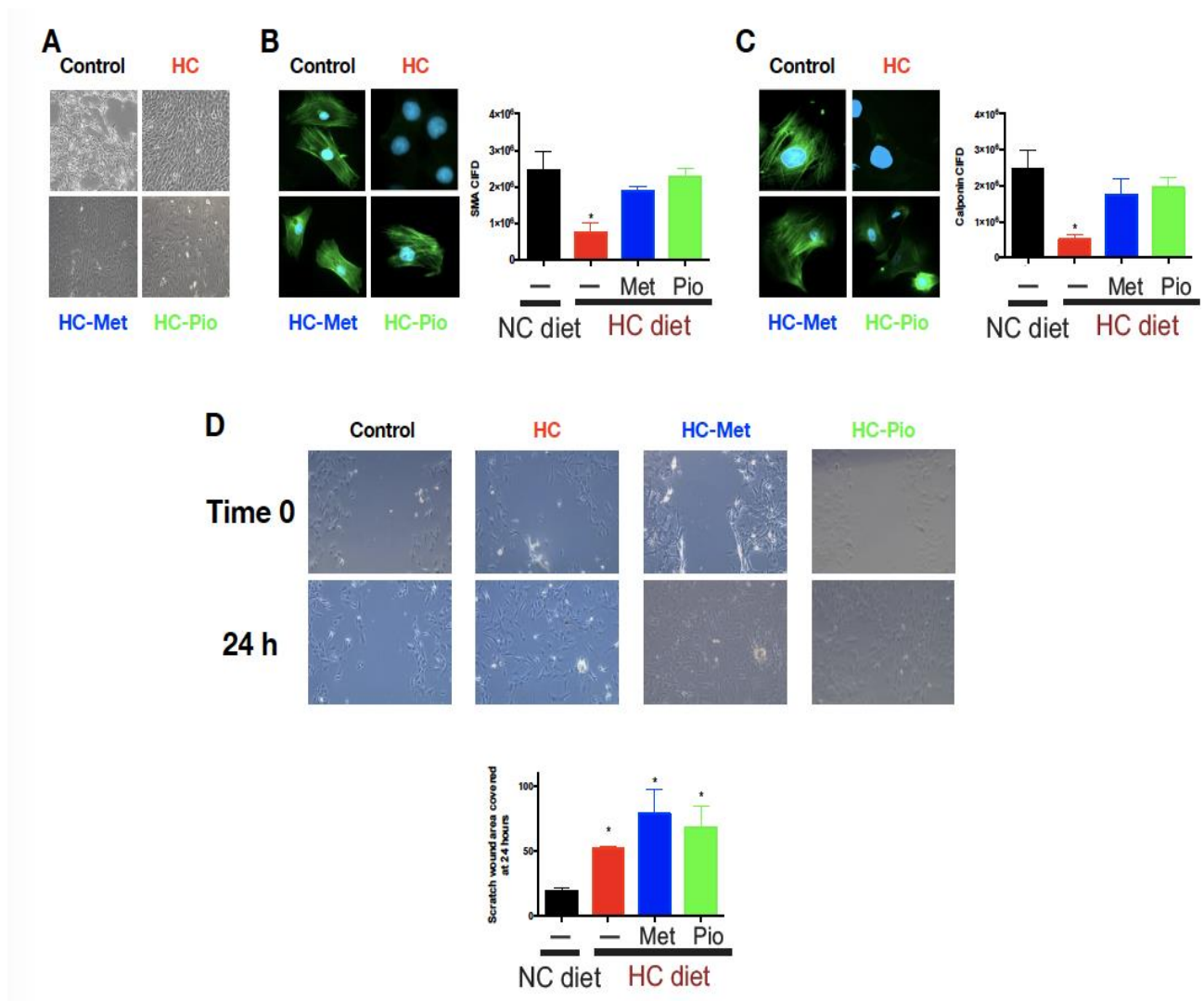
Figure 6. Primary VSMCs from HC-fed exhibit a phenotype reminiscent of a contractile-to-synthetic switch.

A, Light microscope images of VSMCs from 12 week control, HC, metformin, and pioglitazone rats; B, Representative α-SMA immunofluorescence images of VSMCs from 12 week control, HC, metformin, and pioglitazone rats (left). Quantified immunofluorescence results (mean fluorescence intensity ± SEM, n=5) (right); C, Representative calponin immunofluorescence images of VSMCs from 12 week control, HC, metformin, and pioglitazone rats (left). Quantified immunofluorescence results (mean fluorescence intensity ± SEM, n=5) (right); D, Representative scratch assay images at 0 and 24 hours after scratch, of VSMCs from 12 week control, HC, metformin, and pioglitazone rats (top). Quantified migration results (mean wound area covered at 24 hours ± SEM, n=5) (bottom). Statistical analysis was done using one-way ANOVA followed by Tukey's multiple comparisons test. * denotes P < 0.05 vs. control.
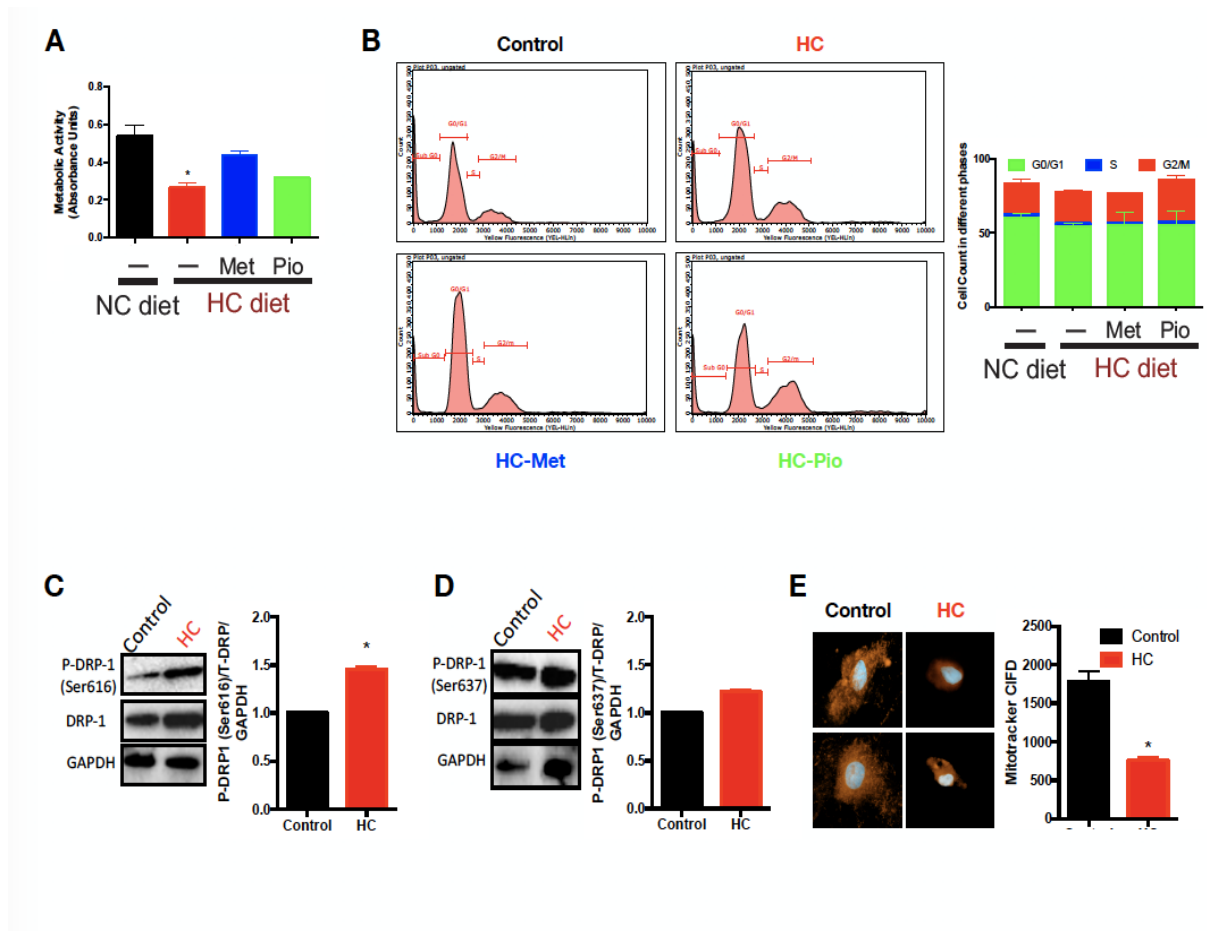
Figure 7. Metabolic changes at the level of VSMCs occur upon twelve weeks of hypercaloric feeding.

A, Metabolic activity of VSMCs isolated from 12 week control, HC, metformin, and pioglitazone rats (mean absorbance units ± SEM, n=4); B, Graphical representation of cell cycle analysis of VSMCs isolated from 12 week control, HC, metformin, and pioglitazone rats (left) and quantification of cell count at different cell cycle stages (mean cell number ± SEM, n=3) (right); C, Representative DRP-1 and P-DRP (Ser616) blots on 12 week control and HC VSMCs (left). Quantified results (mean optical density ± SEM, n=2) (right); D, Representative DRP-1 and P-DRP (Ser637) blots on 12 week control and HC VSMCs (left). Quantified results (mean optical density ± SEM, n=2) (right); E, Representative mitotracker images of individual VSMCs from 12 week control and HC rats (left) and quantified results (mean fluorescence intensity/cell ± SEM, n=3). For A & B, statistical analysis was done using one-way ANOVA followed by Tukey's multiple comparisons test, while unpaired t-test was used for C, D, & E. * denotes $P < 0.05$ vs. control cells.

F. *In vitro* metabolic challenge does not induce inflammation in rat aortic VSMCs

It is possible that hyperinsulinemia and hypertriglyceridemia may be mediating the derogatory effects of HC feeding on the vasculature. In fact, several studies have reported that free fatty acids, including oleate and palmitate, lead to VSMC inflammation and apoptosis (100,101). However, when put to the test, VSMCs challenged with 1600μM free fatty acids (FFAs) and 40 mIU/L insulin (Figure 8A) did not exhibit any changes on MTT assay (Figure 8B), or immunofluorescence imaging for α-SMA and calponin (Figure 8C), indicating that no phenotypic switch occurred. Moreover, metabolic challenge did not alter VSMC chemotactic ability, as evidenced by the equal number of monocytes recruited to control and challenged VSMCs when an adhesion assay was carried out (Figure 8D).

A, *In vitro* stress FFA/Ins

B, Metabolic Activity (Absorbance Units) — Control, 400 µM FFA, 1600 µM FFA

C, Control, HC; SMA CIFD

D, Adherent THP-1 Cells/Unit VSMC area (Cell/1000 µm²) — Control, Ins/FFA
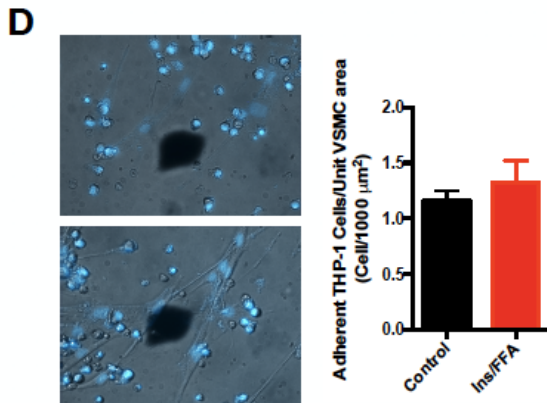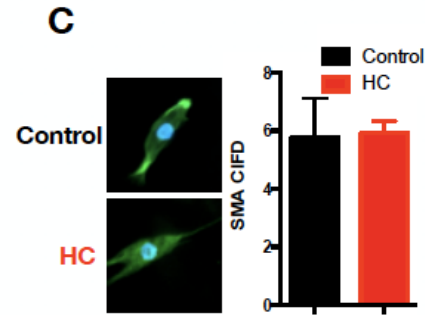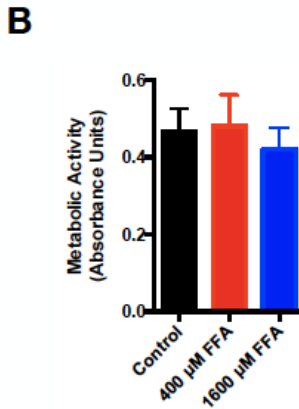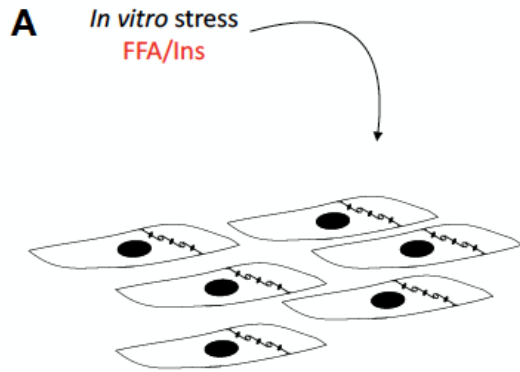
Figure 8. Metabolic Challenge does not induce morphologic nor inflammatory changes in VSMCs.
A, Schematic of the experimental design. Cells depicted are VSMCs; B, Metabolic activity measured using MTT assay in control VSMCs treated with 0, 400, and 1600µM FFAs (mean of absorbance units ± SEM, n=5); Representative α-SMA immunofluorescence images of individual control or metabolically-challenged VSMCs (left). Quantification is on the right (Mean fluorescence intensity per cell ± SEM, n=3); D, Representative images of the cell adhesion assay done on control and metabolically-challenged VSMCs (left). The blue dots in the images represent THP-1 monocyte nuclei. The VSMCs are seen as outlines. Quantified results are to the right (Mean THP-1 cell count per unit VSMC area ± SEM, n=3). For B, statistical analysis was done by one-way ANOVA followed by Tukey's multiple comparisons test, while unpaired t-test was used for C & D. * denotes $P < 0.05$ vs. control cells.

G. Metabolic Stress-Induced VSMC Dysfunction May be Mediated by Adipocyte Inflammation

Since our in vitro model of metabolic stress was not sufficient to induce a VSMC phenotypic switch, which is characteristic of CVD, we attempted to test the role of adipose tissue in mediating this change. This was done by differentiating pre-adipocyte precursor cells to adipocytes (Figure 9A), subjecting them to a 24-hour metabolic challenge, and treating VSMCs with cultured media from this challenge (Figure 9B). Treated VSMCs (24 hour duration) were found to exhibit similar phenotypic changes to primary VSMCs isolated from 12-week HC-fed rats, including a decrease in metabolic activity (Figure 9C) and α-SMA expression (Figure 9D). Further investigations into the causative role of adipocytes in mediating the VSMC phenotypic change were warranted, and since PVAT inflammation was an early phenomenon observed in our HC-fed rat model, we sought to investigate adipocyte inflammation *in vitro*. Firstly, metabolically challenged adipocytes for 24 hours were shown to exhibit greater chemotactic ability, as evidenced by their increased recruitment of THP-1 monocytes in the cell adhesion assay (Figure 10B). This cell-adipocyte coculture was then shown to secrete more TGF-β1 and IL-1β than controls (Figure 10D&E), suggestive of its pro-inflammatory nature and M1 polarization of its macrophages. However, FACS analysis of recruited macrophages revealed that both CD86, a marker of M1 polarization, and CD163, an M2 marker, exist on the surfaces of their cells (Figure 10C). This was initially surprising, but recent articles have identified the existence of macrophages with both CD86 and CD163 markers in certain disease states, which adds to a body of evidence suggesting that the characterization of macrophages into M1/M2 is too simplistic and does not accurately depict *in vivo* processes (58,102). Studying the inflammatory mediators released by these cells is a better indication of

their pro- or anti- inflammatory effects. Interestingly, metabolically-challenged

monocytes did not exhibit increased activation to macrophages, as shown by MTT

assay (Figure 10A), suggesting that the inflammatory cascade begins at the level of the
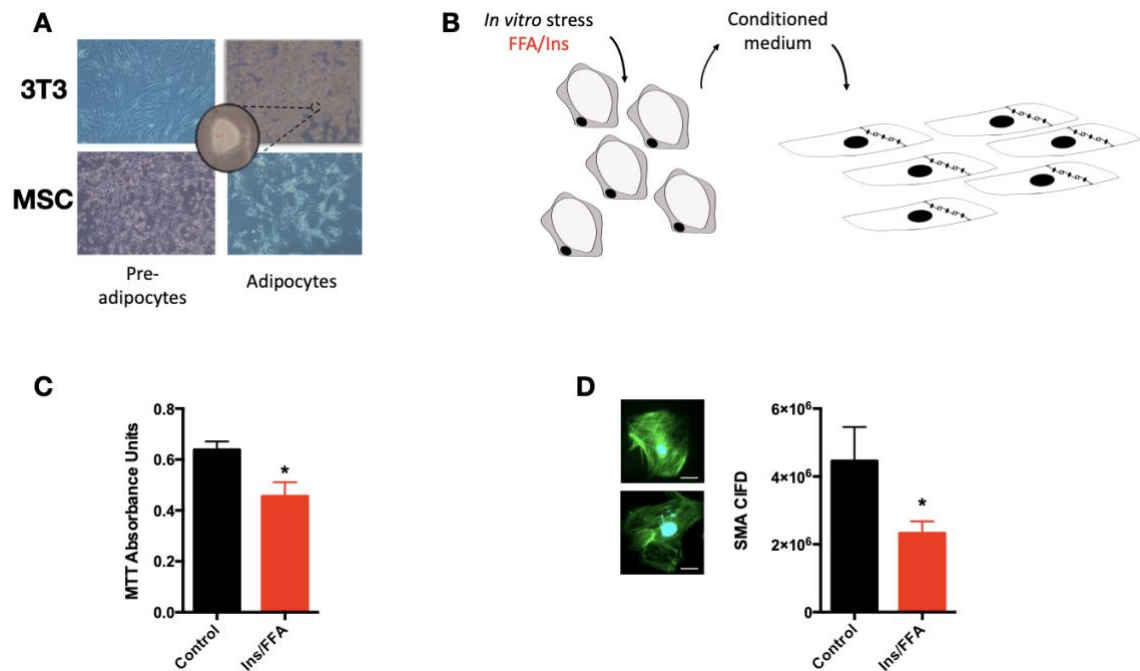
adipocyte.

Figure 9. The in vitro model of metabolic challenge resulted in VSMC phenotypic switching when transduced by adipocytes.

A, Pre-adipocyte and adipocyte cell lines. Top panel: 3T3 fibroblasts and adipocytes derived from them (Left-Right); B, Representative schematic of the experimental protocol; C, MTT absorbance assay on VSMCs treated with stressed-adipocyte conditioned media compared to controls that were treated with conditioned media from control adipocytes (mean absorbance units ± SEM, n=6); Representative α-SMA immunofluorescence images of VSMCs treated with stressed-adipocyte conditioned media compared to those treated with conditioned media from control adipocytes (left). Quantified results are on the right (mean fluorescence intensity ± SEM, n=3). Statistical analysis was carried out using unpaired t-test. * denotes P-value < 0.05 in VSMCs treated with conditioned medium from stressed adipocytes versus from control adipocytes.
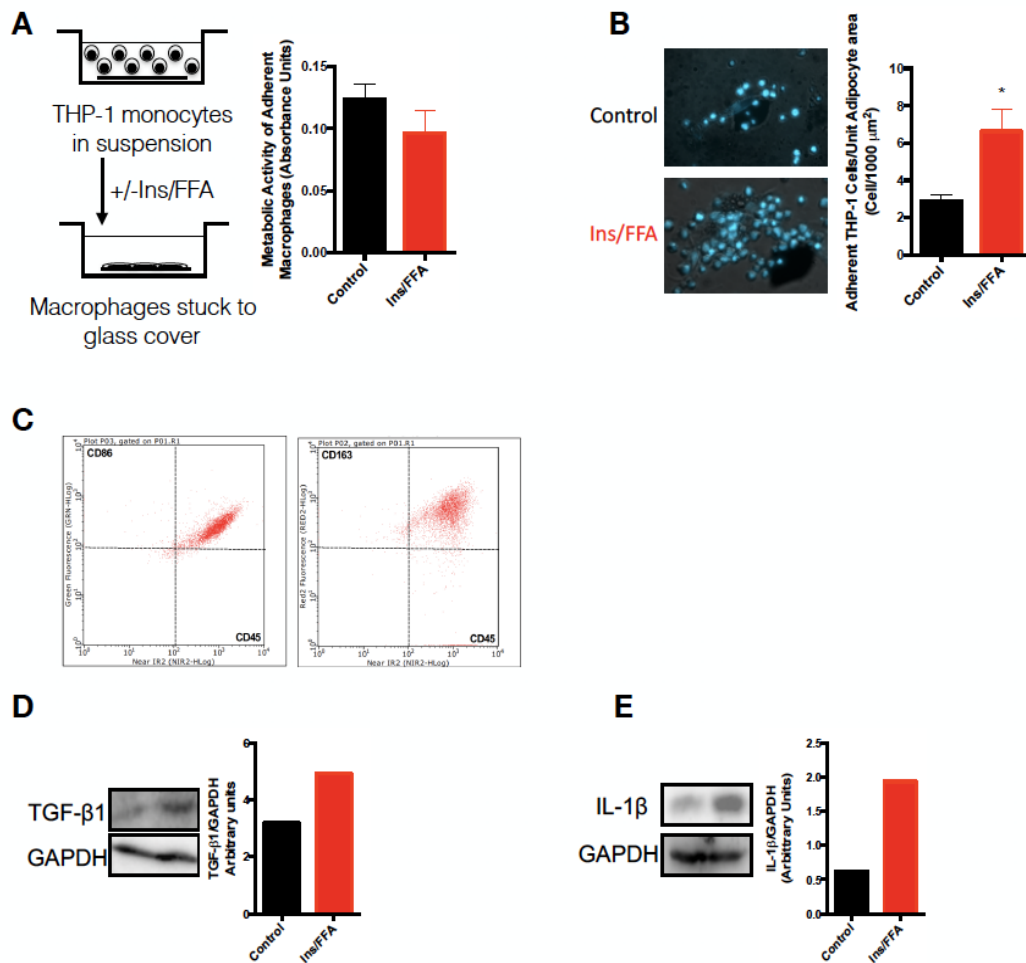
Figure 10. Metabolically Challenged Adipocytes Exhibit a Pro-Inflammatory Phenotype.

A) Schematic of monocyte-to-macrophage differentiation experimental design (left). Quantification of results obtained upon MTT assay to detect monocyte-to-macrophage differentiation upon metabolic challenge versus control (Mean absorbance units ± SEM, n=3) (right); B, Representative images of THP-1 monocyte recruitment assay to control versus metabolically-challenged adipocytes. Blue dots represent macrophage nuclei, while the adipocyte outline can be seen superimposed. Quantification of these results is represented on the right (mean adherent THP-1 cell number per adipocyte area ± SEM, n=3); C, Representative FACS analysis graphs depicting an abundance of CD86+ and CD163+ cell markers; D, Representative TGF-β1 blot done on adipocyte-macrophage coculture using control and metabolically-challenged adipocytes (left). Quantification is on the right (mean optical density ± SEM, n=3); E, Representative IL-1β blot done on adipocyte-macrophage coculture using control and metabolically-challenged adipocytes (left). Quantification is on the right (mean optical density ± SEM, n=3). Statistical analysis was done using unpaired *t*-test. * denotes P < 0.05 versus control cells.

CHAPTER V

DISCUSSION

Our rat model of mild hypercaloric challenge is meant to provide the basis to study the pathophysiological incidents that bring about diabetes and its associated complications in isolation of hyperglycemia and obesity. Focusing on the main killer and one of the earliest established complications of DM (Reference), we aimed to investigate the onset of CVD in this model by characterizing changes in vessel contractility and VSMC phenotype. PVAT inflammation is a known mediator, among others, of vascular dysfunction in atherosclerosis, hypertension, and other vascular disorders. However, little is known about its role in causing early CVD. Moreover, PVAT browning is a phenomenon that is frequently overlooked in the transition from normoglycemia to dysglycemia, and its role in the development of cardiovascular disease is poorly characterized. We thus assessed whether changes in PVAT inflammatory profile and beige adipocyte content occur in our HC model. In addition, we examined whether metabolic stress that leads to localized PVAT inflammation is sufficient to instigate early VSMC phenotypic switching. This was done by studying the effects of this metabolic challenge on the adipocyte-VSMC signaling axis in vitro. Our model of mild hypercaloric intake has proven to cause PVAT inflammation in the absence of systemic inflammation or hyperglycemia. Furthermore, vessels from metabolically-challenged rats exhibited a hypercontractile state when studied using myobath experiments. Aortic VSMCs cultured from MHC-fed rats displayed a contractile-to-synthetic switch, which was paralleled in control VSMCs treated with media conditioned by metabolically challenged adipocytes. However, metabolically challenged VSMCs failed to exhibit the same phenotypic switch, which is suggestive of

61

a direct, causative role played by the adipocyte in the establishment of early VSMC dysfunction that metabolic challenge cannot cause independently.

The HFD animal model was initially developed in order to study the early effects of T2DM in the context of its natural development due to unfavorable dietary habits (103). In a mouse model of impaired glucose tolerance and T2DM, C57BL/6J mice developed hyperglycemia after a single week of consuming a HFD of 58% fat composition, providing an efficient method by which to investigate early diabetes (104). However, this timeline of diabetes development exaggerates the natural history of the disease in humans, and ignores the important stages of pathophysiology developed before dysglycemia and obesity. The HFD model has been modified with various fat composition profiles ranging from 40-60%, with time until the induction of dysglycemia varying accordingly (105). In order to have a reasonable timeframe in which to study the pathophysiology leading to obesity and prediabetes, our HC model receives 38% of its energy intake as fat, which is slightly higher than the 20-35% fat intake that the ADA recommends (106). Moreover, in order to more accurately simulate the Western diet that has been associated with diabetes development (62), fructose was selected as the main choice of carbohydrate, due to its abundance in carbonated beverages, corn syrup additives, and prepared foods (107,108). Studies have shown that a HFD enriched with fructose produces similar or worsened cardiovascular dysfunction but earlier, more robust dysglycemia, and an increase in triglyceride levels that is not observed in HFD fed rats alone (109,110). Our 38% fat, fructose-enriched HC diet provides an extra Calorie (kilocalorie) per gram of chow compared to control, and produces sustained fasting hyperglycemia at 16 weeks of hypercaloric feeding, providing ample time for investigations into pre-hyperglycemic pathology. Moreover,

HC rat body weight does not vary after 12 weeks of feeding, indicating that any observed changes in cardiovascular function or PVAT morphology occur independently of obesity or altered body mass index (BMI). Therefore, the effects of metabolic challenge that are being assessed at 12 weeks of MHC feeding are exhibited systemically solely at the level of hyperinsulinemia and an elevated blood triglyceride and non-HDL cholesterol profile.

It is worth noting that although MHC rats did not differ in terms of weight gain, a change in body composition involving an increase in the ratio of fat to lean tissue was observed on magnetic resonance imaging (MRI). Body composition analysis is increasingly being utilized in humans as a more sensitive measure for detecting obesity than anthropometric measures such as BMI (111). As for animals, Woods et al. noted that rats fed a 40% fat diet for 10 weeks displayed a 10% increase in total body weight but a 35-40% increase in total body fat compared to those fed a low-fat diet, indicating that body composition is a more sensitive criterion for the early detection of obesity even in animals (112). However, no cutoff point has been set in terms of body composition for what constitutes an obese phenotype in rats. The increase in fat to lean ratio of ~25% observed in our model is an expected phenomenon due to the expansion of adipose tissue depots in order to accommodate the increase in calories that HC rats are fed. Moreover, it is safe to assume that these rats have not entered the pathological phase of adipose tissue expansion that involves a surge in hypoxic and inflammatory mediators, due to the lack of change in TGF-β and IL-1β expression in the epididymal fat pad as evidenced by PCR, despite an increase in epididymal fat mass. The epididymal fat pad in rats is a white adipose tissue depot that is known to incur hypoxic expansion in obesity, and whose removal in a model of HFD-fed rats reduced plasma

pro-inflammatory cytokine levels (113). In addition, obesity in humans is associated with a plasma increase in inflammatory mediators, including IL-1β and TGF-β (114,115), and ELISA assays carried out on rat sera indicated that our model does not exhibit elevated levels of IL-1β and TGF-β, further suggesting that changes in cardiovascular function elicited by the HC diet occur pre-obesity.

Changes at the level of PVAT, however, were not so subtle. Oil Red-O staining done on PVAT sections displayed an increase in the size of lipid droplets, indicating hypertrophy of existing adipocytes, which was associated with hypoxia as evidenced by the increase in HIF1α detected by western blot. This change in PVAT morphology has previously been reported in models of HFD-induced obesity, where PVAT mass and adipocyte size were found to be increased in the context of hypoxic injury (116,117). However, an important difference between the HFD findings and our model is the lack of increase in PVAT mass at 12 weeks of HC feeding. This may be explained by the upregulation of UCP-1 observed in PVAT of HC-fed rats, suggesting that browning of white adipocytes is occurring, which favors the oxidation of lipids as opposed to their storage, generating energy in the form of heat instead of lipids in the form of mass. One may speculate that this mechanism peaks at a certain time before decompensating and transitioning into an increase in PVAT mass. In fact, evidence from the Framingham heart study suggests that periaortic fat volume not only increases in obesity, but is also correlated with higher thoracic aorta dimensions, likely playing a role in obesity-induced vascular remodeling (118). The absence of an increase in PVAT mass in our model is in stark contrast to the gain in WAT observed in the form of an increase in epididymal fat mass. Even more striking is the fact that epididymal fat, which has undergone significant expansion in terms of mass, expresses the same amount of IL-1β

and TGF-β as control, while PVAT exhibits a myriad of pro-inflammatory molecules including NF-kB, IL-1β, and TGF-β. While one would assume that browning of adipose tissue, as reported in the literature, is beneficial for vascular health, this fact is seemingly at odds with the increase in inflammatory mediators observed in PVAT, compared to their lack thereof in WAT. We hypothesize that the identity of PVAT as a beige hybrid adipose tissue confers it with limited expandability, which forces it to undergo browning as a restricted, primary mechanism to counter increased caloric intake, a mechanism that is quickly accompanied by hypertrophy that is comparatively small but sufficient to induce hypoxia. Additional studies need to be carried out to test this hypothesis.

Our model of HC-induced metabolic challenge has propelled a pro-inflammatory phenotype in PVAT along multiple planes, including an elevation in P-IKKβ - NF-kB - IL1β pathway expression, increased recruitment of CD68+ macrophages, and increased TGF-β expression. It has been established that the NF-kB pathway is a principal regulator of inflammation downstream of caloric excess both in adipose and other tissues, and plays a fundamental role in instigating insulin resistance (119). IKKβ is one of two kinases that are involved in the regulation of NF-kB transcription. Normally present inactive in the cytoplasm, phosphorylation of IKKβ induces the activation of its kinase domain, which it uses to phosphorylate inhibitors complexed to NF-kB, leading to their dissociation and the subsequent translocation of NF-kB to the nucleus. Once there, NF-kB transcribes inflammatory cytokines including IL-1β that play a direct role in mediating insulin resistance by acting on insulin receptor substrate 1 (IRS-1) (120). TGF-β also plays an important role in the pathogenesis of obesity by influencing the release of inflammatory mediators and promoting remodeling

and collagen deposition in adipose tissue. TGF-β is said to mediate its role through different signaling pathways depending on the adipose tissue depot in question, with Smad3, PAI-1, and ERK1/2 and Akt implicated in different depots (121). However, TGF-β signaling has been understudied in PVAT, and the signaling pathway that predominates in this tissue has yet to be discovered. The fact that two inflammatory cascades that usually characterize inflammation in obesity and diabetes are upregulated so early on in metabolic challenge in PVAT is suggestive of this tissue's important role in mediating early prediabetic pathology.

Peroxisome proliferator activated receptor-γ (PPAR-γ) is a transcription factor known to characterize adipose tissue and is implicated in adipocyte differentiation, lipogenesis, and the maintenance of an anti-inflammatory M2 phenotype in PVAT macrophages. The decrease in the expression of this transcription factor in HC-fed rats supports our hypothesis that a detrimental switch from M2 to M1 is occurring in PVAT. Moreover, it is known that one of the mechanisms by which HIF-1α leads to a decrease in adiponectin expression is decreasing PPARγ through the activation of the PI3K-Akt pathway (64). It is thus possible that the production of adiponectin, a known vasodilator, is downregulated in our model, which is a mechanism by which vascular function may be impaired.

After establishing the prevalence of PVAT dysfunction in our model, we aimed to investigate whether this finding is paralleled at the level of the vasculature, by assessing thoracic aortic inflammation using immunohistochemistry and western blot to detect TGF-β1 and IL-1β expression levels, respectively. Both cytokines were found to be elevated, which not only signifies an increase in inflammation at the level of the vasculature, but also implies that active remodeling that could impact cardiovascular

function is taking place (121). This is because both TGF-β1 and IL-1β converge at the ERK1/2 signaling pathway, which is known to be involved in vascular remodeling, and was indeed shown to be elevated in our model. The increase in aortic thickness observed on hematoxylin and eosin (H&E) staining might be attributed to ERK1/2 activation (99). In addition, TGF-β1 and IL-1β may mediate vascular impairment through the induction of ROS, which was shown to be elevated in our model (99). It is important to note, however, that CD68+ macrophage recruitment to the thoracic aorta was not present in HC-fed rats. This is in contrast to the remarkable increase in CD68+ macrophages forming crown-like structures around adipocytes in HC-fed rat PVAT, which indicates that PVAT inflammation precedes that of the aorta in the timeline of prediabetic pathology. This is because cytokine production is required to mediate an increase in immune cell recruitment, and therefore temporally precedes the latter.

It is now apparent that vessel inflammation and remodeling exist in the aortas of HC-fed rats. However, what this means at the functional level is still elusive, so we conducted myobath experiments on thoracic aortic rings in order to assess contractile function in response to the administration of phenylephrine, a known vasoconstrictor. Not surprisingly, vessels from HC-fed rats exhibited an exaggerated response to phenylephrine a state that was extrapolated into an augmented pressor response to phenylephrine administered *in vivo*. Indeed, this hypercontractile state was previously reported in another pre-diabetic rat model, the Goto-Kakizaki rat. However, the latter study did not examine the role of PVAT inflammation. Vascular hypercontractility is a significant observation in this context, given that it is well-documented that inflamed PVAT loses its capacity to act as a vasorelaxant, by upregulating vasoconstrictive

adipokines including visfatin and chemerin, and decreasing the production of vasodilatory agents including adiponectin (81).

Cardiovascular diseases that manifest at the level of the whole vessel usually begin within the cell, with aberrations affecting one or more cell type and leading to a cumulative change that is observable in terms of disease. VSMCs are the stromal cells and contractile machinery of the vessel wall, and their dual identity confers upon them a plasticity that enables them to switch from a contractile to synthetic state during disease conditions (122). The presence of this synthetic state in our rat model would verify the existence of extensive vascular damage early on in diabetic pathology and justify the use of aggressive therapeutic strategies in order to prevent this switch. In order to investigate this, thoracic aortic VSMCs were isolated, cultured, and subjected to different assays in order to characterize their proliferative, migratory, and contractile capacity. Firstly, morphological changes between the control and HC groups were apparent, with control cells exhibiting a spindle-shaped morphology that is characteristic of contractile cells, and those from HC-fed rats appearing rhomboid and occupying less space per cell, suggesting that de-differentiation from a highly specialized contractile phenotype has occurred. These findings were supported by immunofluorescence staining to detect alpha-smooth muscle actin, which was down-regulated in cells from HC-fed rats. This is in congruence with the characterization of de-differentiated VSMCs as reported in the literature, with variation in the cytoskeleton of these cells not limited to alpha smooth muscle actin, but also including a global reorganization of myosin and intermediate filaments so that the cell shape itself is altered from spindle-shaped to rhomboid.

It is worth noting that VSMCs involved in the phenotypic switch in CVD are characterized by an increase in proliferative and migratory capacity that is required for the processes of wound healing, stable atheroma formation, and neointimal thickening in pathogenic states. In order to study these parameters in our model, we utilized 3-(4,5-dimethylthiazol-2-yl)-2,5-diphenyltetrazolium bromide (MTT) and scratch assays for proliferation and migration respectively. A scratch assay, or wound healing assay, is a commonly utilized tool for studying cell migration, in which portions of a cell monolayer are scratched off and the ability of cells to migrate to "heal" the scratched area is measured (123). Although HC-fed rat VSMCs displayed increased migratory capacity, which is in accordance with the events of the phenotypic switch, their proliferative capacity did not match. The proliferative profile of a phenotypically switched VSMC was absent, as evidenced by the decrease in metabolic activity observed on MTT assays. Furthermore, because MTT assays measure proliferation by assessing the capacity of the cell to reduce MTT to formazan, a capacity that is augmented with an increase in mitochondrial oxidoreductases, a decrease in VSMC metabolic activity on MTT could either mean that there is a decrease in proliferation or an impairment in mitochondrial activity (124). We thus carried out propidium iodide (PI) staining in order to stratify cells according to their stage in the cell cycle, and comparable results between control and HC-fed groups indicated that the difference in MTT results was not due to proliferation.

Follow-up studies to detect changes in DRP-1 and P-DRP1 indicated that mitochondrial fission was occurring in the progression from control to HC-fed groups, as evidenced by the differentially increased phosphorylation of DRP-1 at Ser616. Further studies using mitotracker orange, a mitochondrial dye that stains these

organelles in a manner that is dependent on membrane potential, revealed not only a decrease in mitochondrial activity in VSMCs from HC-fed rats, but also a reduction of mitochondrial networks and a lack of mitochondrial clustering. Chalmers et al. studied mitochondrial dynamics in VSMC proliferation and noted that mitochondria take on a more diverse architecture in proliferative VSMCs, ranging from small spheres to networks. Moreover, blockade of DRP1-dependent mitochondrial fission by mitochondrial division inhibitor-1 (mdivi-1) prevented VSMC proliferation, indicating that mitochondrial fission may be an essential step in modulating VSMC phenotypic switch (35). Moreover, phosphorylation of DRP-1 at Ser616, which increases its GTPase activity and enhances mitochondrial fission was shown to be upregulated by Cdk1/cyclinB, a pro-mitotic cyclin-dependent kinase, indicating that mitochondrial fission is required for cell proliferation (125). Thus, the increase in mitochondrial fission observed in VSMCs from HC-fed rats may indicate that the cell is transitioning into a more proliferative state, even though it is not quite there yet. If so, our study would be the first to outline that proliferation is the last in a sequence of de-differentiating events that comprise the VSMC phenotypic switch. However, there exists an alternative explanation for these findings, because mitochondrial dysfunction is implicated in cell senescence (126,127). The presence of senescent VSMCs was documented in atheromatous plaques and may be implicated in atheroma de-stabilization. However, VSMC senescence usually occurs at late stages of atherosclerosis, distant from the timeline our model is studying. Moreover, VSMC senescence is associated with a chemotactic response that recruits immune cells, which was not observed in our model (127), making it unlikely that VSMC senescence is taking place in our model.

Thus far, the discussion regarding cardiovascular dysfunction has mainly included characterization of early cardiovascular dysfunction in HC-fed rats. However, we attempted to address the pharmacological question that was posed when two trials showed a beneficial effect of metformin and pioglitazone on cardiovascular dysfunction prior to the onset of hyperglycemia (92,94), by investigating whether these drugs might exhibit their therapeutic benefit by modulating PVAT inflammation. Firstly, metformin and pioglitazone treatment exhibited a partial or complete restoration of most HC-induced CVD, notably at the level of vessel contractility. At the level of PVAT inflammation, these drugs were shown to decrease the expression of inflammatory mediators, including NF-kB, IL-1β, and TGF-β1. However, in order for a causal relationship to be established, in vitro studies must be conducted that directly assess the role of these drugs in modulating the adipocyte-VSMC signaling axis, which we plan to conduct in the future.

We hypothesized upon initiation of this study that PVAT inflammation may be playing an early role in the instigation of CVD in prediabetes. After demonstrating that PVAT inflammation and CVD coincide in a manner that suggests temporal precedence of PVAT inflammation in a model of HC-fed rats, we aimed to establish whether a causative role exists for PVAT in the mediation of vascular dysfunction. This is by adopting an in vitro model of PVAT by differentiating two pre-adipocyte cell lineages, 3T3-L1 fibroblasts and human bone marrow mesenchymal stem cells (BMMSCs) into adipocytes. 3T3-L1 fibroblasts are a murine cell line are a well-established model for studying adipogenesis and obesity in vitro, and BMMSCs are capable of adipocytic differentiation in vivo (128,129). Upon differentiation of these cells, they were exposed to 1600μM of a 2:1 ratio of the free fatty acids (FFAs) oleate and palmitate and

40mIU/L of insulin, mimicking the levels of these components in the sera of HC-fed rats. Conditioned medium from these cells was then used to stress rat thoracic aortic and human subcutaneous VSMCs, 3T3-L1 medium used for the former and BMMSC for the latter. Changes at the level of metabolic activity and α-SMA expression that were similar to those in VSMCs isolated from HC-rats were documented, suggesting that the causative agent for the phenotypic switch observed in these primary cells is secreted by challenged adipocytes into their culture medium.

Furthermore, VSMCs subjected the same metabolic challenge exhibited no changes in proliferation or α-SMA expression, indicating that adipocytes are required to mediate the dysfunction observed. Thus far, adipocytes alone have demonstrated the capability to induce a phenotypic switch in VSMCs upon metabolic challenge. However, we were interested in studying the chemotactic ability of challenged adipocytes, in order to characterize whether the change in adipocyte secretory capacity observed is coupled with a pro-inflammatory component. To this end, we utilized THP-1 cells, a human monocytic cell line derived from an acute monocytic leukemia (AML) patient, in a cell adhesion assay in order to assess whether metabolically-challenged adipocytes recruit more monocytes. Our results showed that indeed they do, in line with in vivo work that describes increased expression of monocyte chemoattractant protein 1 (MCP-1) and macrophage inflammatory protein 1α (MIP-1α) in inflamed PVAT (81). Interestingly, challenged VSMCs did not display an increase in chemotactic ability, which is similar to what our work showed with regards to CD68 recruitment in inflamed PVAT versus aorta. In order to further characterize the inflammatory profile of recruited monocytes, and in an effort to assess their M2/M1 polarization, we used fluorescent associated cell sorting (FACS) for CD86 and CD163, markers of the M1 and M2

macrophage cell lineage, respectively. Surprisingly, the recruited monocytes appeared to express both markers. However, western blots done on the coculture revealed an increased expression of the inflammatory cytokines IL-1β and TGF-β1 in the metabolically challenged group, in parallel with our findings in the HC model. Future directions include assessing whether one of these cytokines plays a role in the observed VSMC phenotypic switch, by using selective inhibitors of their function including the TGF-β1 pathway inhibitor, SB431542, that works by inhibiting ALK4, ALK5, and ALK7 that act downstream of TGF-β1. TGF-β1 is a likely contender due to its possible role in suppressing myocardin expression through the Smad3 pathway, which we have shown to be overexpressed in the aortas of HC-fed rats (130). Myocardin is a master regulator of smooth muscle gene expression, including α-SMA and calponin, and its downregulation in VSMCs could mediate the phenotypic switch observed in HC-fed rats (131).

A main limitation of our study is that the question of metabolic stress-induced endothelial dysfunction was not addressed as a possible mediator of VSMC phenotypic switch. Endothelial cells both are exposed to the luminal content that was shown to be altered in terms of lipid composition and play a major role in vascular function through myoendothelial feedback. However, given the lack of CD68+ cell recruitment that was observed in vascular tissues frim HC, a direct endothelial contribution to the inflammatory phenotype is unlikely. However, future studies involving the *in vitro* interaction between human umbilical vein endothelial cells (HUVECs) and VSMCs are underway to provide direct evidence.

In this study, we demonstrated that inflammatory changes in PVAT occur early on in a model of metabolic challenge leading to diabetes. This PVAT inflammation,

though observed in isolation of hyperglycemia, hypertension, and obesity, was accompanied by inflammatory and functional changes at the level of vessels and vascular smooth muscle cells. Using an *in vitro* model of metabolic challenge, our study showed that challenged adipocytes can induce similar detrimental vascular changes to those observed *in vivo*, thus indicating that early PVAT inflammation might serve as an instigator of the initial vascular deterioration in the course of diabetes development. As such, the present results implicate the adipocyte as a main player in the transduction of early metabolic challenge into vascular dysfunction.

REFERENCES

1. American Diabetes Association. Diagnosis and classification of diabetes mellitus. Diabetes Care. 2010 Jan;33 Suppl 1:S62-69.

2. Emerging Risk Factors Collaboration, Sarwar N, Gao P, Seshasai SRK, Gobin R, Kaptoge S, et al. Diabetes mellitus, fasting blood glucose concentration, and risk of vascular disease: a collaborative meta-analysis of 102 prospective studies. Lancet. 2010 Jun 26;375(9733):2215–22.

3. Kaiser AB, Zhang N, Der Pluijm WV. Global Prevalence of Type 2 Diabetes over the Next Ten Years (2018-2028). Diabetes. 2018 May;67(Supplement 1):202-LB.
4. Davies JC, Alton EWFW, Bush A. Cystic fibrosis. BMJ. 2007 Dec 15;335(7632):1255–9.

5. Rowley WR, Bezold C, Arikan Y, Byrne E, Krohe S. Diabetes 2030: Insights from Yesterday, Today, and Future Trends. Popul Health Manag. 2017;20(1):6–12.

6. Boyle JP, Honeycutt AA, Narayan KMV, Hoerger TJ, Geiss LS, Chen H, et al. Projection of Diabetes Burden Through 2050: Impact of changing demography and disease prevalence in the U.S. Diabetes Care. 2001 Nov 1;24(11):1936–40.

7. Bergman M, Buysschaert M, Schwarz PE, Albright A, Narayan KV, Yach D. Diabetes prevention: global health policy and perspectives from the ground. Diabetes Manag (Lond). 2012;2(4):309–21.

8. Gregg EW, Li Y, Wang J, Burrows NR, Ali MK, Rolka D, et al. Changes in diabetes-related complications in the United States, 1990-2010. N Engl J Med. 2014 Apr 17;370(16):1514–23.

9. Wändell PE. Quality of life of patients with diabetes mellitus. An overview of research in primary health care in the Nordic countries. Scand J Prim Health Care. 2005 Jun;23(2):68–74.

10. Trikkalinou A, Papazafiropoulou AK, Melidonis A. Type 2 diabetes and quality of life. World J Diabetes. 2017 Apr 15;8(4):120–9.

11. Redekop WK, Koopmanschap MA, Stolk RP, Rutten GEHM, Wolffenbuttel BHR, Niessen LW. Health-related quality of life and treatment satisfaction in Dutch patients with type 2 diabetes. Diabetes Care. 2002 Mar;25(3):458–63.

12. Low Wang CC, Hess CN, Hiatt WR, Goldfine AB. Clinical Update: Cardiovascular Disease in Diabetes Mellitus: Atherosclerotic Cardiovascular Disease and Heart Failure in Type 2 Diabetes Mellitus – Mechanisms, Management, and Clinical Considerations. Circulation. 2016 Jun 14;133(24):2459–502.

13.	Grundy SM, Benjamin IJ, Burke GL, Chait A, Eckel RH, Howard BV, et al. Diabetes and Cardiovascular Disease: A Statement for Healthcare Professionals From the American Heart Association. Circulation. 1999 Sep 7;100(10):1134–46.

14.	Duckworth W, Abraira C, Moritz T, Reda D, Emanuele N, Reaven PD, et al. Glucose Control and Vascular Complications in Veterans with Type 2 Diabetes. New England Journal of Medicine. 2009 Jan 8;360(2):129–39.

15.	Effects of Intensive Glucose Lowering in Type 2 Diabetes. New England Journal of Medicine. 2008 Jun 12;358(24):2545–59.

16.	Heller SR, on behalf of the ADVANCE Collaborative Group. A Summary of the ADVANCE Trial. Diabetes Care. 2009 Nov 1;32(suppl_2):S357–61.

17.	Fowler MJ. Microvascular and Macrovascular Complications of Diabetes. Clinical Diabetes. 2008 Apr 1;26(2):77–82.

18.	Atkinson MA. The pathogenesis and natural history of type 1 diabetes. Cold Spring Harb Perspect Med. 2012 Nov 1;2(11).

19.	Foulis AK. Pancreatic pathology in type 1 diabetes in human. Novartis Found Symp. 2008;292:2–13; discussion 13-18, 122–9, 202–3.

20.	Guillausseau P-J, Meas T, Virally M, Laloi-Michelin M, Médeau V, Kevorkian J-P. Abnormalities in insulin secretion in type 2 diabetes mellitus. Diabetes Metab. 2008 Feb;34 Suppl 2:S43-48.

21.	Röder PV, Wu B, Liu Y, Han W. Pancreatic regulation of glucose homeostasis. Exp Mol Med. 2016 Mar 11;48:e219.

22.	Bansal N. Prediabetes diagnosis and treatment: A review. World J Diabetes. 2015 Mar 15;6(2):296–303.

23.	Marso SP, Daniels GH, Brown-Frandsen K, Kristensen P, Mann JFE, Nauck MA, et al. Liraglutide and Cardiovascular Outcomes in Type 2 Diabetes. New England Journal of Medicine. 2016 Jul 28;375(4):311–22.

24.	Zinman B, Wanner C, Lachin JM, Fitchett D, Bluhmki E, Hantel S, et al. Empagliflozin, Cardiovascular Outcomes, and Mortality in Type 2 Diabetes. New England Journal of Medicine. 2015 Nov 26;373(22):2117–28.

25.	Rask-Madsen C, King GL. Vascular complications of diabetes: mechanisms of injury and protective factors. Cell Metab. 2013 Jan 8;17(1):20–33.

26.	An X-R, Li X, Wei W, Li X-X, Xu M. Prostaglandin E1 Inhibited Diabetes-Induced Phenotypic Switching of Vascular Smooth Muscle Cells Through Activating Autophagy. Cell Physiol Biochem. 2018;50(2):745–56.

27.	Zhang X, Wang X, Zhou X, Ma X, Yao Y, Liu X. Phenotypic transformation of smooth muscle cells from porcine coronary arteries is associated with connexin 43. Mol Med Rep. 2016 Jul;14(1):41–8.

28.	Bennett MR, Sinha S, Owens GK. Vascular Smooth Muscle Cells in Atherosclerosis. Circ Res. 2016 Feb 19;118(4):692–702.

29.	Etienne P, Parés-Herbuté N, Monnier L, Rabesandratana H, Mani-Ponset L, Gabrion J, et al. Phenotype modulation in primary cultures of aortic smooth muscle cells from streptozotocin-diabetic rats. Differentiation. 1998 Aug;63(4):225–36.

30.	Bochaton-Piallat M-L, Ropraz P, Gabbiani F, Gabbiani G. Phenotypic Heterogeneity of Rat Arterial Smooth Muscle Cell Clones: Implications for the Development of Experimental Intimal Thickening. Arteriosclerosis, Thrombosis, and Vascular Biology. 1996 Jun;16(6):815–20.

31.	Chiong M, Cartes-Saavedra B, Norambuena-Soto I, Mondaca-Ruff D, Morales PE, GarcÃa-Miguel M, et al. Mitochondrial metabolism and the control of vascular smooth muscle cell proliferation. Frontiers in Cell and Developmental Biology [Internet]. 2014 Dec 15 [cited 2019 May 13];2. Available from: http://journal.frontiersin.org/article/10.3389/fcell.2014.00072/abstract

32.	Parra V, Verdejo H, del Campo A, Pennanen C, Kuzmicic J, Iglewski M, et al. The complex interplay between mitochondrial dynamics and cardiac metabolism. J Bioenerg Biomembr. 2011 Feb;43(1):47–51.

33.	Chang C-R, Blackstone C. Dynamic regulation of mitochondrial fission through modification of the dynamin-related protein Drp1. Ann N Y Acad Sci. 2010 Jul;1201:34–9.

34.	Taguchi N, Ishihara N, Jofuku A, Oka T, Mihara K. Mitotic phosphorylation of dynamin-related GTPase Drp1 participates in mitochondrial fission. J Biol Chem. 2007 Apr 13;282(15):11521–9.

35.	Chalmers S, Saunter C, Wilson C, Coats P, Girkin JM, McCarron JG. Mitochondrial motility and vascular smooth muscle proliferation. Arterioscler Thromb Vasc Biol. 2012 Dec;32(12):3000–11.

36.	Siasos G, Tsigkou V, Kosmopoulos M, Theodosiadis D, Simantiris S, Tagkou NM, et al. Mitochondria and cardiovascular diseases-from pathophysiology to treatment. Ann Transl Med. 2018 Jun;6(12):256.

37.	American Diabetes Association. Diagnosis and Classification of Diabetes Mellitus. Diabetes Care. 2014 Jan 1;37(Supplement_1):S81–90.

38.	DeFronzo RA, Abdul-Ghani M. Assessment and treatment of cardiovascular risk in prediabetes: impaired glucose tolerance and impaired fasting glucose. Am J Cardiol. 2011 Aug 2;108(3 Suppl):3B-24B.

39.   Hopper I, Billah B, Skiba M, Krum H. Prevention of diabetes and reduction in major cardiovascular events in studies of subjects with prediabetes: meta-analysis of randomised controlled clinical trials. European Journal of Cardiovascular Prevention & Rehabilitation. 2011 Dec;18(6):813–23.

40.   Emanuela F, Grazia M, Marco DR, Maria Paola L, Giorgio F, Marco B. Inflammation as a Link between Obesity and Metabolic Syndrome. Journal of Nutrition and Metabolism. 2012;2012:1–7.

41.   Brannick B, Dagogo-Jack S. Prediabetes and Cardiovascular Disease. Endocrinology and Metabolism Clinics of North America. 2018 Mar;47(1):33–50.
42.   Dagogo-Jack S, Askari H, Tykodi G. Glucoregulatory physiology in subjects with low-normal, high-normal, or impaired fasting glucose. J Clin Endocrinol Metab. 2009 Jun;94(6):2031–6.

43.   Toft-Nielsen MB, Damholt MB, Madsbad S, Hilsted LM, Hughes TE, Michelsen BK, et al. Determinants of the impaired secretion of glucagon-like peptide-1 in type 2 diabetic patients. J Clin Endocrinol Metab. 2001 Aug;86(8):3717–23.

44.   Mather KJ, Funahashi T, Matsuzawa Y, Edelstein S, Bray GA, Kahn SE, et al. Adiponectin, change in adiponectin, and progression to diabetes in the Diabetes Prevention Program. Diabetes. 2008 Apr;57(4):980–6.

45.   Kanat M, DeFronzo RA, Abdul-Ghani MA. Treatment of prediabetes. World J Diabetes. 2015 Sep 25;6(12):1207–22.

46.   Yan F, Cha E, Lee ET, Mayberry RM, Wang W, Umpierrez G. A Self-assessment Tool for Screening Young Adults at Risk of Type 2 Diabetes Using Strong Heart Family Study Data. Diabetes Educ. 2016;42(5):607–17.

47.   Knight JA. Diseases and disorders associated with excess body weight. Ann Clin Lab Sci. 2011;41(2):107–21.

48.   Giordano A, Kay Song C, Bowers RR, Christopher Ehlen J, Frontini A, Cinti S, et al. Reply to Kreier and Buijs: no sympathy for the claim of parasympathetic innervation of white adipose tissue. American Journal of Physiology-Regulatory, Integrative and Comparative Physiology. 2007 Jul 1;293(1):R550–2.

49.   Giordano A, Song CK, Bowers RR, Ehlen JC, Frontini A, Cinti S, et al. White adipose tissue lacks significant vagal innervation and immunohistochemical evidence of parasympathetic innervation. Am J Physiol Regul Integr Comp Physiol. 2006 Nov;291(5):R1243-1255.

50.   Rousset S, Alves-Guerra M-C, Mozo J, Miroux B, Cassard-Doulcier A-M, Bouillaud F, et al. The Biology of Mitochondrial Uncoupling Proteins. Diabetes. 2004 Feb 1;53(Supplement 1):S130–5.

51.   Rosell M, Kaforou M, Frontini A, Okolo A, Chan Y-W, Nikolopoulou E, et al. Brown and white adipose tissues: intrinsic differences in gene expression and response to cold exposure in mice. Am J Physiol Endocrinol Metab. 2014 Apr 15;306(8):E945-964.

52.   Enerbäck S. Human Brown Adipose Tissue. Cell Metabolism. 2010 Apr;11(4):248–52.

53.   Qi X-Y, Qu S-L, Xiong W-H, Rom O, Chang L, Jiang Z-S. Perivascular adipose tissue (PVAT) in atherosclerosis: a double-edged sword. Cardiovasc Diabetol. 2018 10;17(1):134.

54.   Weisberg SP, McCann D, Desai M, Rosenbaum M, Leibel RL, Ferrante AW. Obesity is associated with macrophage accumulation in adipose tissue. J Clin Invest. 2003 Dec;112(12):1796–808.

55.   Shaul ME, Bennett G, Strissel KJ, Greenberg AS, Obin MS. Dynamic, M2-like remodeling phenotypes of CD11c+ adipose tissue macrophages during high-fat diet--induced obesity in mice. Diabetes. 2010 May;59(5):1171–81.

56.   Roth M. Faculty of 1000 evaluation for Exocytosis of macrophage lysosomes leads to digestion of apoptotic adipocytes and foam cell formation. [Internet]. 2016 [cited 2019 May 16]. Available from: http://f1000.com/prime/726266297#eval793519183

57.   Murano I, Barbatelli G, Parisani V, Latini C, Muzzonigro G, Castellucci M, et al. Dead adipocytes, detected as crown-like structures, are prevalent in visceral fat depots of genetically obese mice. Journal of Lipid Research. 2008 Jul;49(7):1562–8.

58.   Trombetta AC, Soldano S, Contini P, Tomatis V, Ruaro B, Paolino S, et al. A circulating cell population showing both M1 and M2 monocyte/macrophage surface markers characterizes systemic sclerosis patients with lung involvement. Respir Res. 2018 Sep 24;19(1):186.

59.   Trayhurn P, Beattie JH. Physiological role of adipose tissue: white adipose tissue as an endocrine and secretory organ. Proc Nutr Soc. 2001 Aug;60(3):329–39.

60.   Meyer C, Dostou JM, Welle SL, Gerich JE. Role of human liver, kidney, and skeletal muscle in postprandial glucose homeostasis. Am J Physiol Endocrinol Metab. 2002 Feb;282(2):E419-427.

61.   Sun K, Kusminski CM, Scherer PE. Adipose tissue remodeling and obesity. J Clin Invest. 2011 Jun;121(6):2094–101.

62.   Arner P, Arner E, Hammarstedt A, Smith U. Genetic predisposition for Type 2 diabetes, but not for overweight/obesity, is associated with a restricted adipogenesis. PLoS ONE. 2011 Apr 12;6(4):e18284.

63.   Gealekman O, Guseva N, Hartigan C, Apotheker S, Gorgoglione M, Gurav K, et al. Depot-Specific Differences and Insufficient Subcutaneous Adipose Tissue Angiogenesis in Human Obesity. Circulation. 2011 Jan 18;123(2):186–94.

64.   Ye J. Emerging role of adipose tissue hypoxia in obesity and insulin resistance. Int J Obes (Lond). 2009 Jan;33(1):54–66.

65.   McArdle MA, Finucane OM, Connaughton RM, McMorrow AM, Roche HM. Mechanisms of Obesity-Induced Inflammation and Insulin Resistance: Insights into the Emerging Role of Nutritional Strategies. Frontiers in Endocrinology [Internet]. 2013 [cited 2019 May 16];4. Available from: http://journal.frontiersin.org/article/10.3389/fendo.2013.00052/abstract

66.   Surmi BK, Hasty AH. Macrophage infiltration into adipose tissue: initiation, propagation and remodeling. Future Lipidol. 2008;3(5):545–56.

67.   Chung K-J, Chatzigeorgiou A, Economopoulou M, Garcia-Martin R, Alexaki VI, Mitroulis I, et al. A self-sustained loop of inflammation-driven inhibition of beige adipogenesis in obesity. Nature Immunology. 2017 Jun;18(6):654–64.

68.   Chalkiadaki A, Guarente L. High-Fat Diet Triggers Inflammation-Induced Cleavage of SIRT1 in Adipose Tissue To Promote Metabolic Dysfunction. Cell Metabolism. 2012 Aug;16(2):180–8.

69.   Hui X, Zhang M, Gu P, Li K, Gao Y, Wu D, et al. Adipocyte SIRT1 controls systemic insulin sensitivity by modulating macrophages in adipose tissue. EMBO reports. 2017 Apr;18(4):645–57.

70.   Saraswathi V, Hasty AH. The role of lipolysis in mediating the proinflammatory effects of very low density lipoproteins in mouse peritoneal macrophages. Journal of Lipid Research. 2006 Jul;47(7):1406–15.

71.   Anderson EK, Hill AA, Hasty AH. Stearic Acid Accumulation in Macrophages Induces Toll-Like Receptor 4/2-Independent Inflammation Leading to Endoplasmic Reticulum Stress–Mediated Apoptosis. Arteriosclerosis, Thrombosis, and Vascular Biology. 2012 Jul;32(7):1687–95.

72.   Shi H, Kokoeva MV, Inouye K, Tzameli I, Yin H, Flier JS. TLR4 links innate immunity and fatty acid–induced insulin resistance. Journal of Clinical Investigation. 2006 Nov 1;116(11):3015–25.

73.   Pedersen DJ, Guilherme A, Danai LV, Heyda L, Matevossian A, Cohen J, et al. A major role of insulin in promoting obesity-associated adipose tissue inflammation. Mol Metab. 2015 Jul;4(7):507–18.

74.   Xu X, Grijalva A, Skowronski A, van Eijk M, Serlie MJ, Ferrante AW. Obesity Activates a Program of Lysosomal-Dependent Lipid Metabolism in Adipose Tissue

Macrophages Independently of Classic Activation. Cell Metabolism. 2013 Dec;18(6):816–30.

75.   Coats BR, Schoenfelt KQ, Barbosa-Lorenzi VC, Peris E, Cui C, Hoffman A, et al. Metabolically Activated Adipose Tissue Macrophages Perform Detrimental and Beneficial Functions during Diet-Induced Obesity. Cell Rep. 2017 Sep 26;20(13):3149–61.

76.   Bluher M. Adipose tissue inflammation: a cause or consequence of obesity-related insulin resistance? Clinical Science. 2016 Aug 8;130(18):1603–14.

77.   Szasz T, Bomfim GF, Webb RC. The influence of perivascular adipose tissue on vascular homeostasis. Vasc Health Risk Manag. 2013;9:105–16.

78.   Soltis EE, Cassis LA. Influence of perivascular adipose tissue on rat aortic smooth muscle responsiveness. Clin Exp Hypertens A. 1991;13(2):277–96.

79.   Löhn M, Dubrovska G, Lauterbach B, Luft FC, Gollasch M, Sharma AM. Periadventitial fat releases a vascular relaxing factor. FASEB J. 2002 Jul;16(9):1057–63.

80.   Gao Y-J, Lu C, Su L-Y, Sharma AM, Lee RMKW. Modulation of vascular function by perivascular adipose tissue: the role of endothelium and hydrogen peroxide. Br J Pharmacol. 2007 Jun;151(3):323–31.

81.   Nosalski R, Guzik TJ. Perivascular adipose tissue inflammation in vascular disease. Br J Pharmacol. 2017 Oct;174(20):3496–513.

82.   Tilg H, Moschen AR. Adipocytokines: mediators linking adipose tissue, inflammation and immunity. Nat Rev Immunol. 2006 Oct;6(10):772–83.

83.   Wang P, Xu T-Y, Guan Y-F, Su D-F, Fan G-R, Miao C-Y. Perivascular adipose tissue-derived visfatin is a vascular smooth muscle cell growth factor: role of nicotinamide mononucleotide. Cardiovascular Research. 2009 Feb 1;81(2):370–80.

84.   Oda A, Taniguchi T, Yokoyama M. Leptin stimulates rat aortic smooth muscle cell proliferation and migration. Kobe J Med Sci. 2001 Jun;47(3):141–50.

85.   Huang F, Xiong X, Wang H, You S, Zeng H. Leptin-induced vascular smooth muscle cell proliferation via regulating cell cycle, activating ERK1/2 and NF-kappaB. Acta Biochim Biophys Sin (Shanghai). 2010 May 15;42(5):325–31.

86.   Bohlen F, Kratzsch J, Mueller M, Seidel B, Friedman-Einat M, Witzigmann H, et al. Leptin inhibits cell growth of human vascular smooth muscle cells. Vascul Pharmacol. 2007 Jan;46(1):67–71.

87.   Takaoka M, Nagata D, Kihara S, Shimomura I, Kimura Y, Tabata Y, et al. Periadventitial adipose tissue plays a critical role in vascular remodeling. Circ Res. 2009 Oct 23;105(9):906–11.

88.   Wang Y, Lam KSL, Xu JY, Lu G, Xu LY, Cooper GJS, et al. Adiponectin inhibits cell proliferation by interacting with several growth factors in an oligomerization-dependent manner. J Biol Chem. 2005 May 6;280(18):18341–7.

89.   Fésüs G, Dubrovska G, Gorzelniak K, Kluge R, Huang Y, Luft FC, et al. Adiponectin is a novel humoral vasodilator. Cardiovasc Res. 2007 Sep 1;75(4):719–27.

90.   Hildebrand S, Stümer J, Pfeifer A. PVAT and Its Relation to Brown, Beige, and White Adipose Tissue in Development and Function. Front Physiol. 2018;9:70.

91.   Kong L-R, Zhou Y-P, Chen D-R, Ruan C-C, Gao P-J. Decrease of Perivascular Adipose Tissue Browning Is Associated With Vascular Dysfunction in Spontaneous Hypertensive Rats During Aging. Front Physiol. 2018;9:400.

92.   Diabetes Prevention Program Research Group. Long-term effects of lifestyle intervention or metformin on diabetes development and microvascular complications over 15-year follow-up: the Diabetes Prevention Program Outcomes Study. Lancet Diabetes Endocrinol. 2015 Nov;3(11):866–75.

93.   Mohan M, Al-Talabany S, McKinnie A, Mordi IR, Singh JSS, Gandy SJ, et al. A randomized controlled trial of metformin on left ventricular hypertrophy in patients with coronary artery disease without diabetes: the MET-REMODEL trial. Eur Heart J. 2019 Apr 17;

94.   Kernan WN, Viscoli CM, Furie KL, Young LH, Inzucchi SE, Gorman M, et al. Pioglitazone after Ischemic Stroke or Transient Ischemic Attack. N Engl J Med. 2016 Apr 7;374(14):1321–31.

95.   Qi T, Chen Y, Li H, Pei Y, Woo S-L, Guo X, et al. A role for PFKFB3/iPFK2 in metformin suppression of adipocyte inflammatory responses. J Mol Endocrinol. 2017;59(1):49–59.

96.   Spencer M, Yang L, Adu A, Finlin BS, Zhu B, Shipp LR, et al. Pioglitazone treatment reduces adipose tissue inflammation through reduction of mast cell and macrophage number and by improving vascularity. PLoS ONE. 2014;9(7):e102190.

97.   Reeves PG, Nielsen FH, Fahey GC. AIN-93 Purified Diets for Laboratory Rodents: Final Report of the American Institute of Nutrition Ad Hoc Writing Committee on the Reformulation of the AIN-76A Rodent Diet. The Journal of Nutrition. 1993 Nov 1;123(11):1939–51.

98.   Panth N, Paudel KR, Parajuli K. Reactive Oxygen Species: A Key Hallmark of Cardiovascular Disease. Adv Med. 2016;2016:9152732.

99.   Gurjar MV, Deleon J, Sharma RV, Bhalla RC. Role of reactive oxygen species in IL-1 beta-stimulated sustained ERK activation and MMP-9 induction. Am J Physiol Heart Circ Physiol. 2001 Dec;281(6):H2568-2574.

100.   Wu D, Liu J, Pang X, Wang S, Zhao J, Zhang X, et al. Palmitic acid exerts pro-inflammatory effects on vascular smooth muscle cells by inducing the expression of C-reactive protein, inducible nitric oxide synthase and tumor necrosis factor-α. International Journal of Molecular Medicine. 2014 Dec;34(6):1706–12.

101.   Gouni-Berthold I, Berthold HK, Seul C, Ko Y, Vetter H, Sachinidis A. Effects of authentic and VLDL hydrolysis-derived fatty acids on vascular smooth muscle cell growth. Br J Pharmacol. 2001 Apr;132(8):1725–34.

102.   Mitsi E, Kamng'ona R, Rylance J, Solórzano C, Jesus Reiné J, Mwandumba HC, et al. Human alveolar macrophages predominately express combined classical M1 and M2 surface markers in steady state. Respir Res. 2018 18;19(1):66.

103.   Surwit RS, Kuhn CM, Cochrane C, McCubbin JA, Feinglos MN. Diet-Induced Type II Diabetes in C57BL/6J Mice. Diabetes. 1988 Sep 1;37(9):1163–7.

104.   Winzell MS, Ahren B. The High-Fat Diet-Fed Mouse: A Model for Studying Mechanisms and Treatment of Impaired Glucose Tolerance and Type 2 Diabetes. Diabetes. 2004 Dec 1;53(Supplement 3):S215–9.

105.   Buettner R, Schölmerich J, Bollheimer LC. High-fat Diets: Modeling the Metabolic Disorders of Human Obesity in Rodents*. Obesity. 2007 Apr;15(4):798–808.

106.   Evert AB, Boucher JL, Cypress M, Dunbar SA, Franz MJ, Mayer-Davis EJ, et al. Nutrition Therapy Recommendations for the Management of Adults With Diabetes. Diabetes Care. 2014 Jan 1;37(Supplement_1):S120–43.

107.   Elliott SS, Keim NL, Stern JS, Teff K, Havel PJ. Fructose, weight gain, and the insulin resistance syndrome. Am J Clin Nutr. 2002 Nov;76(5):911–22.

108.   Dornas WC, de Lima WG, Pedrosa ML, Silva ME. Health implications of high-fructose intake and current research. Adv Nutr. 2015 Nov;6(6):729–37.

109.   Huang B-W, Chiang M-T, Yao H-T, Chiang W. The effect of high-fat and high-fructose diets on glucose tolerance and plasma lipid and leptin levels in rats. Diabetes Obes Metab. 2004 Mar;6(2):120–6.

110.   Axelsen LN, Lademann JB, Petersen JS, Holstein-Rathlou N-H, Ploug T, Prats C, et al. Cardiac and metabolic changes in long-term high fructose-fat fed rats with severe obesity and extensive intramyocardial lipid accumulation. American Journal of Physiology-Regulatory, Integrative and Comparative Physiology. 2010 Jun;298(6):R1560–70.

111.   Hariri N, Thibault L. High-fat diet-induced obesity in animal models. Nutrition Research Reviews. 2010 Dec;23(2):270–99.

112.   Woods SC, Seeley RJ, Rushing PA, D'Alessio D, Tso P. A Controlled High-Fat Diet Induces an Obese Syndrome in Rats. The Journal of Nutrition. 2003 Apr 1;133(4):1081–7.

113.   Mulder P, Morrison MC, Wielinga PY, van Duyvenvoorde W, Kooistra T, Kleemann R. Surgical removal of inflamed epididymal white adipose tissue attenuates the development of non-alcoholic steatohepatitis in obesity. International Journal of Obesity. 2016 Apr;40(4):675–84.

114.   Stępień M, Stępień A, Wlazeł RN, Paradowski M, Banach M, Rysz J. Obesity indices and inflammatory markers in obese non-diabetic normo- and hypertensive patients: a comparative pilot study. Lipids Health Dis. 2014 Feb 8;13:29.

115.   Caër C, Rouault C, Le Roy T, Poitou C, Aron-Wisnewsky J, Torcivia A, et al. Immune cell-derived cytokines contribute to obesity-related inflammation, fibrogenesis and metabolic deregulation in human adipose tissue. Scientific Reports [Internet]. 2017 Dec [cited 2019 May 13];7(1). Available from: http://www.nature.com/articles/s41598-017-02660-w

116.   Marchesi C, Ebrahimian T, Angulo O, Paradis P, Schiffrin EL. Endothelial nitric oxide synthase uncoupling and perivascular adipose oxidative stress and inflammation contribute to vascular dysfunction in a rodent model of metabolic syndrome. Hypertension. 2009 Dec;54(6):1384–92.

117.   Ketonen J, Shi J, Martonen E, Mervaala E. Periadventitial adipose tissue promotes endothelial dysfunction via oxidative stress in diet-induced obese C57Bl/6 mice. Circ J. 2010 Jul;74(7):1479–87.

118.   Thanassoulis G, Massaro JM, Corsini E, Rogers I, Schlett CL, Meigs JB, et al. Periaortic adipose tissue and aortic dimensions in the Framingham Heart Study. J Am Heart Assoc. 2012 Dec;1(6):e000885.

119.   Zeng T, Zhou J, He L, Zheng J, Chen L, Wu C, et al. Blocking Nuclear Factor-Kappa B Protects against Diet-Induced Hepatic Steatosis and Insulin Resistance in Mice. Alisi A, editor. PLOS ONE. 2016 Mar 1;11(3):e0149677.

120.   Israël A. The IKK complex, a central regulator of NF-kappaB activation. Cold Spring Harb Perspect Biol. 2010 Mar;2(3):a000158.

121.   Sousa-Pinto B, Gonçalves L, Rodrigues AR, Tomada I, Almeida H, Neves D, et al. Characterization of TGF-β expression and signaling profile in the adipose tissue of rats fed with high-fat and energy-restricted diets. The Journal of Nutritional Biochemistry. 2016 Dec;38:107–15.

122.   Michel J-B, Li Z, Lacolley P. Smooth muscle cells and vascular diseases. Cardiovascular Research. 2012 Jul 15;95(2):135–7.

123.   Liang C-C, Park AY, Guan J-L. In vitro scratch assay: a convenient and inexpensive method for analysis of cell migration in vitro. Nat Protoc. 2007;2(2):329–33.

124.   Sylvester PW. Optimization of the tetrazolium dye (MTT) colorimetric assay for cellular growth and viability. Methods Mol Biol. 2011;716:157–68.

125.   Li H-B, Wang R-X, Jiang H-B, Zhang E, Tan J-Q, Xu H-Z, et al. Mitochondrial Ribosomal Protein L10 Associates with Cyclin B1/Cdk1 Activity and Mitochondrial Function. DNA and Cell Biology. 2016 Nov;35(11):680–90.

126.   Grootaert MOJ, Moulis M, Roth L, Martinet W, Vindis C, Bennett MR, et al. Vascular smooth muscle cell death, autophagy and senescence in atherosclerosis. Cardiovascular Research. 2018 Mar 15;114(4):622–34.

127.   Gardner SE, Humphry M, Bennett MR, Clarke MCH. Senescent Vascular Smooth Muscle Cells Drive Inflammation Through an Interleukin-1α–Dependent Senescence-Associated Secretory Phenotype. Arteriosclerosis, Thrombosis, and Vascular Biology. 2015 Sep;35(9):1963–74.

128.   Ruiz-Ojeda FJ, Rupérez AI, Gomez-Llorente C, Gil A, Aguilera CM. Cell Models and Their Application for Studying Adipogenic Differentiation in Relation to Obesity: A Review. Int J Mol Sci. 2016 Jun 30;17(7).

129.   Abdallah BM. Marrow adipocytes inhibit the differentiation of mesenchymal stem cells into osteoblasts via suppressing BMP-signaling. J Biomed Sci. 2017 Feb 7;24(1):11.

130.   Xie W-B, Li Z, Miano JM, Long X, Chen S-Y. Smad3-mediated myocardin silencing: a novel mechanism governing the initiation of smooth muscle differentiation. J Biol Chem. 2011 Apr 29;286(17):15050–7.

131.   Chen J, Kitchen CM, Streb JW, Miano JM. Myocardin: A Component of a Molecular Switch for Smooth Muscle Differentiation. Journal of Molecular and Cellular Cardiology. 2002 Oct;34(10):1345–56.